R-06-105

# Changes in groundwater composition as a consequence of deglaciation

## Implications for performance assessment

Jordi Guimerà, Lara Duro, Anne Delos
Enviros Spain

November 2006

**Svensk Kärnbränslehantering AB**
Swedish Nuclear Fuel
and Waste Management Co
Box 5864
SE-102 40 Stockholm Sweden
Tel 08-459 84 00
+46 8 459 84 00
Fax 08-661 57 19
+46 8 661 57 19

ISSN 1402-3091
SKB Rapport R-06-105

# Changes in groundwater composition as a consequence of deglaciation

## Implications for performance assessment

Jordi Guimerà, Lara Duro, Anne Delos
Enviros Spain

November 2006

This report concerns a study which was conducted for SKB. The conclusions and viewpoints presented in the report are those of the authors and do not necessarily coincide with those of the client.

A pdf version of this document can be downloaded from www.skb.se

# Abstract

The behaviour of the deep geological repository planned by SKB will depend on the climatic evolution over a long term, such as the advance and retreat of ice sheets after glaciation and deglaciation periods. The melt water enriched in oxygen due to a deglaciation episode will infiltrate into the geological media and may compromise the reducing conditions of the repository. It has been established the importance of microbial activities and oxidation of minerals, such as Fe-bearing minerals to preserve the repository from the oxidant front. Former studies assessed the Fe-bearing mineral capacity to buffer against oxidant conditions due to the intrusion of melt water into the system. The objective of the present study is to update these works using the new data available from the site characterisation. The conceptual model considers a fast flow pathway, characteristic of a fracture into which is introduced melt water equilibrated with atmospheric $O_2$ and $CO_2$. The advance of the oxidant front is kinetically controlled by the dissolution-precipitation of annite (an Fe(II) mica). The alkalinity and the content of aluminium, silica and iron are controlled respectively by the calcite, kaolinite, chalcedony and iron precipitate present into the system. A sensitivity analysis is performed onto the transport and geochemical parameters of the system (flow velocity, porosity, the content of Fe-bearing mineral, the iron-precipitate, reactive surface of the minerals). In the reference case, the oxidant front affects mainly the first five metres of the system over 5,000 years. In the worst case where the flow velocity is important, it reaches 250 metres after 2,000 years. In all cases, the minerals contained in the system control the geochemical changes due to the buffering of the oxidant front.

# Summary


### *Statement of the problem*

The objective of this report is to evaluate in a quantitative fashion some of the effects of the future climatic evolution on the hydrogeochemistry of the granitic environment of the planned SKB repository. Such effects are related to the advance and retreat of ice sheets in sub-polar areas such as the Fennoscandian shield and in particular, the effects of oxygen-rich water infiltration from the melting of ice through geologic media and the effects on the redox condition of the repository.

### *Background*

This work is a further development from previous calculations /Guimerà et al. 1999/ and takes into consideration some of the recommendations by /Gascoyne 1999/. In our previous work we found that oxic conditions – but not oxygen – could reach repository depths under certain circumstances, however, /Gascoyne 1999/ contended that the calculations were excessively conservative and that new data available from site characterization programmes should be used for the pertinent calculations. Hence, we have integrated the actual data arising from the on going site characterisation programmes in this work.

### *Conceptual model*

The conceptual model envisages the system as a fast flowing fracture, were water moves by advection at a "reference" groundwater velocity of $10^{-7}$ m/s. Diluted and oxygen saturated water originated from the melting of ice infiltrates through this fracture and interacts with the main minerals present. These minerals exert control on the alkalinity (calcite), aluminium content (kaolinite) and silica (chalcedony). In addition, the oxidant front is buffered by the kinetic dissolution of ferro-magnesian biotite and the released Fe(III) may precipitate as ferric oxy-hydroxide.

### *Numerical model and results*

The model is solved by means of PHREEQC /Parkhurst and Appelo 1999/. The results of the reference case indicate that the oxygen front only progresses few metres along the fracture. The depletion of the mineral redox capacity in the fracture is able to buffer completely the advance of the oxidizing front. Oxygen does not reach repository depths, where the redox potentials are maintained around –360 mV.

### *Sensitivity analyses*

Sensitivity analyses on the effects of groundwater velocity (from $10^{-5}$ to $10^{-8}$ m/s), mineral redox capacity (annite abundance from 1 to 8 mol/L), reactive surface area (from 1 to 17 $m^2$/L) and on the morphology of the secondary iron(III) precipitates (hematite and amorphous iron hydroxide), also indicate that the system at repository depths maintains reducing conditions (Eh ranging between –180 and –360 mV) under these circumstances.

### *Relevance for performance assessment*

As a consequence of the oxygen intrusion, all components in groundwater are diluted except aluminium and silica. Changes remain within the same order of magnitude for $K^+$ or silica, but differ by more than 4 orders for magnesium. pH increases up to 3 pH units. However, no major changes for the redox state are experienced during the calculated periods. It is worth noting that for any cases analysed, oxygen does not reach repository depths.

# List of notation

| | |
|---|---|
| $\frac{mol_{xx}}{L}$ **[mol·L$^{-1}$]** | XX content per unit of porewater volume |
| **%wt$_{XX}$** | percentage in weight of mineral XX |
| **ϕ [-]** | porosity |
| **ρ [Kg·L$^{-1}$]** | rock bulk density |
| **ν$_{annite}$ [-]** | stoichiometric factor of oxygen in the process of annite oxidation |
| **∇H [-]** | head gradient |
| **Δt [y]** | time step |
| **Δx [m]** | spatial discretisation |
| **A [m$^2$·g$^{-1}$]** | surface area of dissolving mineral per unit of mass |
| **HLRW** | High Level Radioactive Waste |
| **K [m·s$^{-1}$]** | hydraulic conductivity |
| **k$_0$** | neutral constant in the mineral dissolution reaction |
| **K$_{eq}$** | equilibrium constant |
| **k$_H$** | acid constant in the mineral dissolution reaction |
| **k$_{OH}$** | alkaline constant in the mineral dissolution reaction |
| **L$_{GW}$ [L$^3$]** | groundwater volume |
| **m [-]** | alkaline reaction order |
| **M [mol·L$^{-1}$]** | molar concentration units (mol per litre groundwater) |
| **MM$_{XX}$ [Kg·mol$^{-1}$]** | molecular mass of XX |
| **n [-]** | acid reaction order |
| **Pe [-]** | Peclet number |
| **pH$_{pzc}$ [-]** | pH corresponding to the point zero of charge |
| **RDC [mol$_{O2}$·L$^{-1}$]** | reducing capacity |
| **R$_{O2\text{-}infl}$ [mol·L$^{-1}$·s$^{-1}$]** | Rate of oxygen inflow |
| **R$_{XX}$ [mol·m$^{-2}$·y$^{-1}$]** | reaction rate of XX |
| **S$_A$ [m$^2$·L$^{-1}$]** | surface area of dissolving mineral per unit of porewater volume |
| **t$_a$ [y]** | time for oxygen advancement by advection |
| **t$_{ADV}$ [y]** | characteristic time for advection |
| **t$_d$ [y]** | time for oxygen depletion |
| **t$_{OF}$ [y]** | time for oxygen front advancement |
| **t$_{sim}$ [y]** | total time simulated |
| **v [m·s$^{-1}$]** | groundwater velocity |
| **v$_{OF}$ [m·s$^{-1}$]** | velocity of the oxygen front |

# Contents

# 1 Introduction

This chapter provides the framework of the project, within the SR-Can safety assessment being performed by SKB. First, the problem of the ice melting and its implications for performance assessment of deep HLRW disposal are stated. Second, the results of former projects related to this one are presented in the light of their use for the present calculations. The objectives of the report, which broadly refer to the assessment of hydrogeochemical changes induced by deep percolation of oxidizing water, are stated before the description of the methodology proposed to achieve them. Finally, the structure of the report is described.

## 1.1 Background

This report is mostly devoted to assess some particular effects in the hydrogeochemistry of deep hard rocks due to the advance and retreat of ice sheets in sub-polar areas such as the Fennoscandian shield. The development of permafrost is a likely process to occur in similar places and the effects in deep hydrodynamics and thus, in hydrogeochemistry, is notable. This phenomenon is cited for the sake of completeness, but the effects associated are not assessed in detail in this report.

The effects of oxygenated water intrusion in deep hard rocks was early assessed by /Neretnieks 1986/ who analysed the importance of the ferrous minerals to buffer this intrusion by means of analytical solutions. The relevance of the variation of transmissivity in depth, the effect of diffusion of oxygen into the matrix and the availability of ferrous iron where highlighted and in general terms, it was stated that despite the results indicated that oxygenated water could penetrate hundreds of metres in the lifespan of a repository, the current knowledge at that time could not constrain the variability of the parameters to which the calculations were very sensitive. However, it was stated that "the existence of a porous matrix in crystalline rocks has a strong impact on the retardation of many important radionuclides", which was demonstrated by means of the equations provided.

The effects of ice melting and groundwater infiltration in the performance assessment of deep storage of HLRW has progressed during the past decade from the studies of /Blomqvist et al. 1992, Ahonen and Vieno 1994/ or /Boulton and de Marsily 1997/. In general terms, there was a concern that the changes induced by the advance and retreat of ice sheets could jeopardize the geochemical stability of spent fuel. In fact, isotope studies in Finland carried by the first authors pointed to glacial melt water as the most plausible explanation for the isotopic composition of the groundwater samples taken at a depth of 400 m. This induced the second authors to study the effects of glacial water on corrosion of copper canisters. This study first calculated the oxygen content of glacial melt water under different assumptions and obtained that it could be far above the atmospheric pressure equilibrium, up to about 40–45 ppm $O_2$. The hydrodynamics of melt water under the ice sheets was first described by the third authors. In general terms, both hydrodynamics and geochemical calculations were performed in parallel, but they lacked of feed back to each other.

Hence, SITE-94 reported that the concern of deep infiltration of oxidizing waters existed. Thus within SKB-97, /Guimerà et al. 1999/ performed a detailed study of the redox front migration due to deep infiltration of melt water from ice sheets. In this study, a synthesis of the known processes related to the hydrodynamics of ice sheets and the hydrogeology of hard rocks of low permeability was carried out prior to the geochemical model formulation. Consequently, the authors opted for a multicomponent reactive transport approach to assess the evolution of the redox front migration, which was divided into fast flowing fractures and host rock. The buffering capacity of the system was controlled only by iron bearing minerals. /Guimerà et al.

1999/ work was extremely conservative, the only disruptive scenario being the deep storage under a fast flowing fracture and under high hydraulic gradients – fast groundwater velocities – /Glynn and Voss 1999/.

These results, together with a series of literature work, were reviewed by /Gascoyne 1999/ who re-examined the critical factors for the long term maintenance of reducing conditions in a nuclear fuel repository. Among others tasks, this work compares the different oxygen content of ices and ice melt waters, criticises the set of parameters of former studies and evidenced that the flow model of the central scenario of SKB-97 was over simplistic. His review concluded with a firm statement on the potential of the geosphere to act as a barrier against the intrusion of oxidizing water.

More recently, a cooperative effort between SKB and POSIVA crystallised in a synthesis report on the hydrogeochemical stability of groundwaters surrounding a spent nuclear fuel repository in a 100,000 years perspective /Puigdomènech 2001/. They cite the results of the REX project in terms of relevancy for maintaining the reducing conditions of a repository, buffering the intrusion of $O_2$ rich groundwater. This project established the importance of microbial activities for keeping such conditions. "The oxidation of $CH_4$ and $H_2$ was found to be a significant process for $O_2$ reduction /Kotelnikova and Pedersen 1999, Pedersen 2000, Puigdomènech et al. 2001/ which is activated when oxidant waters become mixed with deep groundwaters with emanating reducing gases".

Numerical simulations of groundwater flow, solute transport and bio-chemical reactions was performed by /Samper et al. 2003/. These authors showed, by means of a 1D model, that some of the concentrations of redox-sensitive species – mainly bicarbonate and sulphur – measured during the projects were better reproduced by assuming bacterial activity in the system. This type of results is also put into evidence by many other authors (for example, see /Sidborn 2003/).

The origin and presence of deep saline water in the Baltic and Canadian shields has long been studied. They are attributed to both, the water rock interaction during long residence times and to the deep penetration of residual brines from frozen ocean during glaciations. Also, mixing with more recent and dilute groundwater occurs. The influence of such waters is not considered in this report.

/Luukkonen et al. 2004/ conducted an estimation on which is the effect of the underground excavations in the Olkiluoto bedrock on naturally occurring fracture mineral buffers. Different models were tested by using meteoric water as recharging water type, containing both $O_2$ and inorganic carbon due to the oxidation of organic matter in the soil. In the absence of calcite in the system, pyrite dissolves producing an important pH decrease (from 5.4 to 3.9), while pyrrhotite dissolution produces only minor changes in pH. Both processes consume oxygen thus causing the evolution of the system towards reducing conditions. In the case of assuming that calcite is present, the decrease of pH is buffered, what produces the precipitation of Fe(III) released from the dissolution of iron sulphides.

The results of the simulations presented in /Luukkonen et al. 2004/ are similar to the ones shown in /Guimerà et al. 1999/, where the initial calculations assumed the infiltration of a very low mineralized groundwater (exemplifying glacial melt-water) through a fracture by using the PHREEQC code. In the report /Guimerà et al. 1999/, the influence of different minerals on the buffering of an oxic intrusion was assessed by following two different approaches: i) the stationary state-approach and ii) the equilibrium approach by using the PHREEQC code. Different minerals were assumed to have an effect on the oxygen intrusion: pyrite and Fe-bearing chlorite. The results indicated that in the case of having chlorite in the fractures, the time for the complete depletion of chlorite down to repository depths was over 100,000 years in the worst case of assuming a fast and direct fracture connecting the surface with the repository. Calcite was always able to buffer pH and it was never depleted in the system in the case of assuming that the oxic intrusion was being buffered by chlorite.

The methodology followed in /Luukkonen et al. 2004/ is a good way of assessing general trends of the system regarding to buffering minerals but lack of a more detailed description of some processes that may be of importance. The complexity of the geochemical system should be increased, by incorporating other oxygen consumption processes and pH buffering effects. This is what the work reported in this document has aimed at.

## 1.2 Effects of advance and retreat of ice sheets in deep groundwater circulation

Following, the effects of the advance and retreat of ice sheets are mentioned as main processes affecting the hydrodynamics and geochemistry of groundwater and we explain the deep infiltration of groundwater for its relevancy to this report.

Advance and retreat of ice sheets induce changes on the position of the coast line. Since the coast is the ultimate discharging point of continental groundwater systems, the geometry of the groundwater flow regime is likely to change.

Advance of the ice sheet creates an overpressure which is believed to be responsible for an effect on the deep saline groundwater known as “upconing” /Svensson et al. 2004, Puigdomènech 2001/. Under these circumstances, saline water may migrate upwards and mix with more diluted, recent groundwater as cited before.

The advance of ice sheets also prevents groundwater recharge to happen under normal conditions. Hence, the water budget becomes limited and the groundwater velocities may become reduced; consequently, increased residence times will occur.

On the contrary, during the retreat of ice sheets, water resulting from ice melting infiltrates. Deep infiltration of melt water is the crucial phenomenon that occurs that is pertinent for this report. Recharge may occur under special circumstances yet, despite it is likely to flow and circulate at atmospheric pressure, due to the presence of the basal moraines, locally, sub-glacial water pressures are close to ice overburden pressures /Fountain 1994/. That such overburden pressure is exerted over the whole melt water is quite an assumption, often argued in performance assessment exercises.

/Gascoyne 1999/ collected published compositions of melt ice and ice from different glaciers of polar areas and alpine glaciers. After this collection, he concludes that the calculated composition of 45 ppm $O_2$ by /Ahonen and Vieno 1994/ hardly occurs in natural conditions. On the contrary, despite the cold and high pressure conditions at which gas is entrapped in ice, melt water rarely exceeds 10 ppm $O_2$. Only young ice from the Arolla glacier in the Alps showed contents up to 30 ppm, but more often the same glacier shows contents well below saturation, around 3.5 ppm $O_2$.

This value differs by an order of magnitude to the one used by /Guimerà et al. 1999/ for their modelling calculations. On the one hand, such difference is minor in terms of redox potential; on the other hand, it implies much less oxidants entering into the system. This point has been addressed in the new calculations presented in this report.

The redox front migration of melt ice is buffered by the reducing capacity (RDC) of the system. This RDC was considered to be formed by iron(II) bearing minerals in the former calculations by /Guimerà et al. 1999/. Particularly, pyrite, biotite and chlorite dissolution was considered to be the main source of electron donors. This largely complicated the calculations, since the kinetic expression of dissolution depended on pH, which created high non linearities.

However, recent studies have demonstrated the relevance of microbe population in deep groundwater systems as cited before. As a matter of fact, microbes have been even found in entrapped water bubbles in ice well above frozen Antarctic lakes /Priscu et al. 1999/.

Therefore, it is likely that the presence of microbes enhances the capacity of the system to buffer a redox front. As we will discuss later, calculations done in this report considered that this supplemental need of buffering should be included whenever needed to demonstrate that geochemical system solely is not strong enough to slow the progression of the oxidants intrusion.

The occurrence of the deep infiltration greatly depends on the suitable hydraulic conditions to occur, that is, the redox front will progress preferentially along the fast flowing fractures and less efficiently along the fractured rock mass. The conceptual model for groundwater flow and solute transport has also progressed from the early SITE-94 to the current project. In short, groundwater is envisaged to flow along fast flowing features and a minor portion through connected minor fractures cross-cutting the rock mass. Solutes are transported in turn, by advection and dispersion, but it is recognised that they also diffuse into the stagnant zones close to the flowing features. Accordingly, they experience geochemical reactions depending on the solute and the solid characteristics.

The calculations performed by /Guimerà et al. 1999/ were over-conservative in some cases, and implied the use of certain parameter combinations that were unrealistic at the scales of the model domain. For instance, velocities of $10^{-5}$ m/s were considered in the most pessimistic cases along a domain of 400 m. /Gascoyne 1999/ suggested the use of more realistic values with resulting travel times according to the observations that arise from site investigations.

## 1.3 Objectives of this report

The main objective of this report is to assess the chemical composition of groundwater at depths relevant for deep disposal of HLRW during an episode of ice melting.

Particular objectives are to assess the penetration of the redox front created by the ice melting and the changes in the buffering capacity of the system under different hypotheses.

## 1.4 Methodology

The work performed by /Guimerà et al. 1999/ is the starting point of this project. We start by reviewing the conceptual model formulated and to assess the validity of the geochemical model stated. The definition of RDC of the system is also reviewed in the light of some of the inputs by /Gascoyne 1999/.

A base case conceptual model is formulated and the corresponding equations introduced in a multicomponent reactive transport code. Finally, a sensitivity analysis is performed and the results are discussed.

## 1.5 Structure of this document

The next chapter describes the conceptual model formulation and discusses the hypotheses and restrictions used for such a complex system. Geochemical as well as hydrodynamic assumptions are taken into consideration. Chapter 3 describes the code used for calculation, the structure of the models and the implementation of the conceptual model into the numerical model. Also, numerical sensitivity analyses are described in this chapter. Chapter 4 is dedicated to the results obtained from the calculations for the different systems considered. Finally, Chapter 5 compares the results with former calculations by /Guimerà et al. 1999/ and the document ends up with a summary and conclusions of the project.

# 2 Conceptual model

This chapter describes how we address the effect of ice melt water infiltrated in deep fractured formations. First, a description of the geochemical system is provided, progressing form the pertinent data taken from published literature on the mineralogy of fracture filling materials, to glacial melt waters as well as the mineralogy that controls the redox capacity (RDC) of the system. Second, the relevant issues regarding the hydrodynamics of the problem are discussed and the most relevant assumptions and simplifications, put in the context of the actual site characterisation knowledge, are described. Finally, arising form the discussion from former sections, a description of the base case selected for simulation is provided consisting on the coherent combination of pertinent model dimensions, size and parameters.

## 2.1 System definition

The definition of the system used in the present report is similar to that presented in /Guimerà et al. 1999/. Some of the explanations will not be repeated here, but only the basic assumptions in terms of main processes acting in the system.

According to the objectives, the interest of this project is the assessment of the evolution of the composition of ice-melting water during a de-glaciation period when it infiltrates through a crystalline media. The main focus is on the evolution of the oxygen concentration in the system, considered as the main oxidizing agent due to the higher oxygen fugacity in ice melting water in comparison with surface groundwaters.

Therefore, from a conceptual point of view, the following processes will be considered in the system:

- Infiltration of water resulting from the process of ice melting.
- Interaction of ice-melting water with fracture filling minerals and:
  - subsequent solute acquisition driven by the undersaturation of the ice-melting water with regards to the main minerals present in the system,
  - consumption of oxygen of the infiltrating water due to the presence of minerals with reducing capacity in the media.

A more detailed definition of the system can be seen in /Guimerà et al. 1999/, nevertheless, the sketch used in that report is repeated here for the sake of clarity in the presentation of the system (see Figure 2-1).

In Figure 2-1 it is assumed a repository depth of 500 m below ground. This figure shows that the rock mass – either rock or fracture – is divided into two zones, one with groundwater with Eh > 400 mV and another one with Eh < –100 mV which is reducing. In /Guimerà et al. 1999/ this division was quite arbitrary both in terms of dimensions (100 and 400 m respectively) and Eh. But it helped the numerical models to converge. Hence, infiltration water oversaturated in oxygen entered first in a zone which redox potential was higher than the domain of interest, but lower than the infiltrating water. In doing so, the contrast of the redox potential of waters was lower and the numerical convergence of the calculations speeded up.

In this report, infiltration water is equilibrated with oxygen, and enters into a reducing domain of 400 m depth, for comparison with the former project. This is further discussed in subsequent sections and chapters.

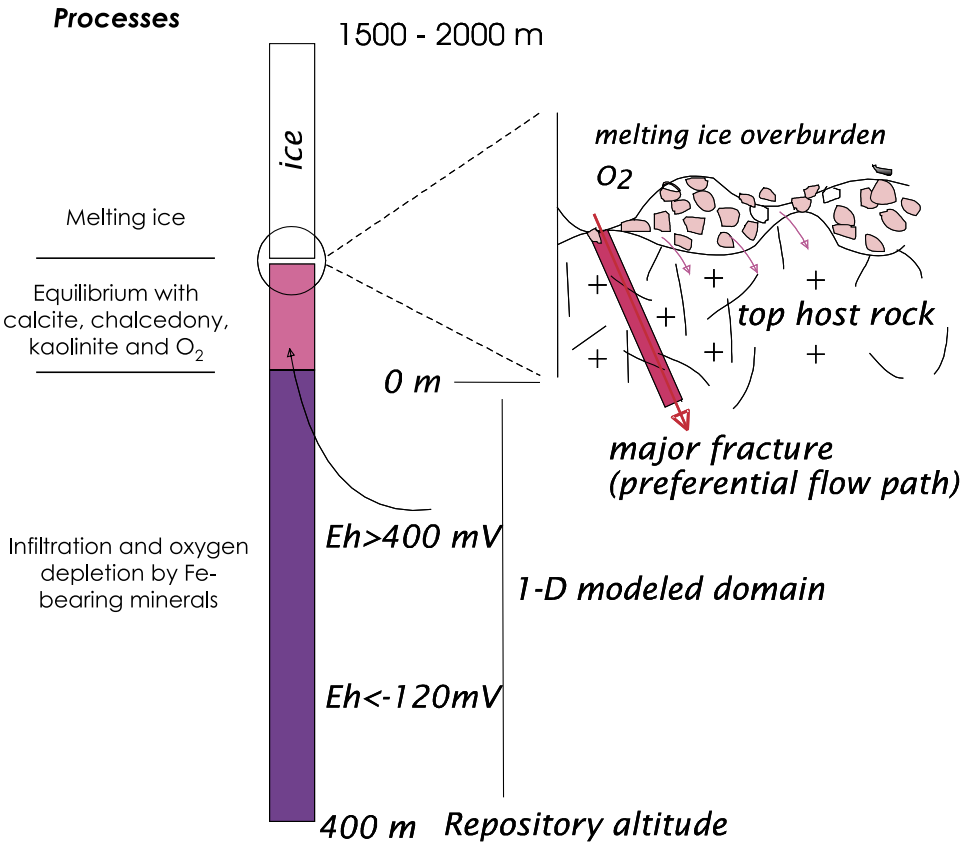


***Figure 2-1.*** *Conceptual model scheme /Guimerà et al. 1999/. The ice overburden is viewed as pressure exerted on top of the modelled domain (prescribed head). Ice melts and water infiltrates first through the top host rock, where redox conditions are oxidant (Eh > 400 mV). Thus, groundwater flows downwards through the modelled domain whose initial redox state is reducing (Eh < –120 mV)*

## 2.2 Geochemical system

Following we conduct a review of the geochemical information available on the Forsmark study site, whose data constitute the baseline of the geochemical system of the model.

### 2.2.1 Mineralogical data

#### *a) Fracture mineralogy*

/Petersson et al. 2004/ analysed the mineralogy of fracture filling and rocks of 4 drill-cores from Forsmark. The dominant fracture minerals in the Forsmark area are quartz, albite, K-feldspar, epidote, prehnite, laumonite, analcime, apophyllite, pyrite, hematite, chlorite, calcite, fluorite, mixed-layer clays, corrensite, illite and saponite. Chlorite, epidote, corrensite and pyrite are minerals providing reducing capacity due to their content in ferrous iron. Chlorite is a common fracture-filling mineral in all fracture sets analysed in tunnels excavated in the Forsmark areas /Carlsson and Christiansson 1987/. Pyrite and epidote are especially found in open fractures, whereas hematite and corrensite are mainly found in fracture coatings. The amount of hematite is relatively low.

All samples are rich in iron, especially the fracture coatings, which represents an important redox buffer along the flow path. Ratios of Fe(II)/Fe(III) have not been measured yet. Other redox sensitive element is manganese, but it is present in very low amounts in the system.

### *b) Rock matrix mineralogy*

The petrographical characterisation from different samples of several boreholes /Petersson et al. 2004/ gives some information on the rock matrix modal composition. The most common rock found in the analysed boreholes is metagranite-granodiorite. The reducing capacity minerals present in this rock matrix are biotite (0.6–10%wt), chlorite (some traces up to 2.4%wt), hornblende (it is found only in few samples, but its amount could rise up to 50%wt) and epidote (some traces up to 1.6%wt). The percentage of Fe(II) in the rock matrix is reported in the range 1.3–2%wt.

A possible fracture description (Figure 2-2) is suggested by /Widestrand et al. 2003/.

### *c) Reducing capacity*

By and large, Fe(II)-bearing aluminosilicates and sulphides are the main source of reductants. Furthermore microbes may also use $CH_4$ and organic carbon to consume $O_2$. Microbial activity in the top soil layer would increase the reducing capacity of the far-field. Biotic processes have been considered in the assessment of the oxygen consumption in the near field of the repository /Grandia et al. 2005/, nevertheless we have not included microbial activity in this study given the uncertainty associated to the quantification of its effect in a system presenting such a high degree of heterogeneity. According to /Puigdomènech et al. 2001/, the major sources of reduction capacity in the system are ferrous silicates and sulphide minerals. Accordingly, the main reactive minerals considered are calcite and Fe-bearing minerals. The mineral composition found in /Petersson et al. 2004/ and /Dershowitz et al. 2003/ is shown in Table 2-1.

The biotite series are minerals of stoichiometric formulae: $K(Fe^{II},Mg)_3AlSi_3O_{10}(OH)_2$, whose two end-members are:

Mg-end member: Phlogopite: $KMg_3AlSi_3O_{10}(OH)_2$

Fe-end member: Annite, $KFe^{II}_3AlSi_3O_{10}(OH)_2$

**Table 2-1. Selected mineral composition of the Forsmark system (%wt, from /Dershowitz et al. 2003/ and /Petersson et al. 2004/).**

| Mineral | Rock matrix | Fracture [3] |
|---|---|---|
| Biotite and chlorite | 1.3–2 [1] | 2 to 20 [2] |
| Calcite | 0.2 to 0.4 | 14.4 |

[1] %wt. Fe(II). [2] as $\%Fe_2O_3$. [3] Including fracture coating.

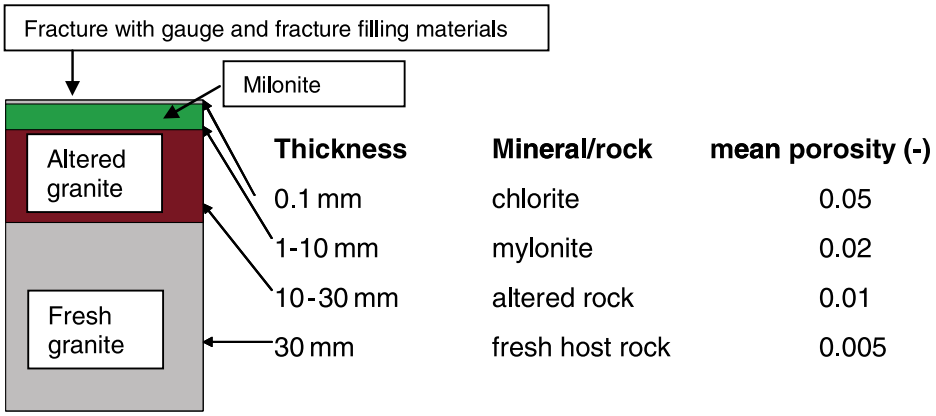


***Figure 2-2.*** *Hypothetical example of fracture layer description from /Widestrand et al. 2003/. Most of groundwater flows through the upper and thinner part of the scheme. Note the presence of electron donors in this part.*

For the sake of simplicity, in this work, annite is considered as the main mineral providing reducing capacity to the system, assuming that the reported biotite is in the ferrous form. The dissolution reaction of annite presented below shows the contribution of Fe(II) to the system.

$KFe^{II}_3AlSi_3O_{10}(OH)_2 + 10H_2O = K^+ + 3Fe^{2+} + Al(OH)_4^- + 3H_4SiO_4 + 6OH^-$

Fe(II) is oxidized by oxygen into Fe(III), which precipitates into iron(III) oxides or hydroxides. For the sake of the calculations we will assume as a reference case the formation of the amorphous Fe(III) hydroxide:

$Fe^{2+} + 0.25\ O_2 + 2.5\ H_2O = Fe(OH)_3(s) + 2H^+$

Al(III) and $H_4SiO_4$ resulting also from the dissolution of annite may form quartz and/or kaolinite.

$2H_4SiO_4 + 2Al^{3+} + H_2O = Al_2Si_2O_5(OH)_4 + 6H^+$

According to the description of the fracture mineralogy in former paragraphs, Table 2-2 summarises the concentration of annite (mol/L) in the system depending on the $Fe_2O_3$ content (assuming that all iron in the fracture filling minerals is Fe(II)) and the porosity considered. Estimated porosities are 0.1 and 0.5 for fracture coating and gouge respectively, 0.02 for mylonite and 0.008 ± 0.002 for the altered rock /Widestrand et al. 2003, Berglund and Selroos 2004/ (p 85 Table 6-1)). Two different fracture porosities have been considered for the calculation of the mineral concentrations: the lowest (0.1) and medium (0.2) fracture porosity. Mylonite porosity has been selected for the rock matrix.

Annite abundance is estimated in Table 2-2 as follows:

First, we can estimate the iron content (mol/L) in the $Fe_2O_3$ present in Forsmark fracture – reported by /Dershowitz et al. 2003/ and /Petersson et al. 2004/ – from the bulk rock density ($\rho = 2.7$ kg/L), the molecular mass of $Fe_2O_3$ ($MM_{Fe2O3} = 160$ g/mol) and the porosity ($\phi$) of the fracture (either 0.1 or 0.2):

$$\frac{mol_{Fe}}{L} = \%wt_{Fe_2O_3} \cdot \frac{\rho}{MM_{Fe_2O_3}} \cdot \frac{2\,mol_{Fe}}{1\,mol_{Fe_2O_3}} \cdot \frac{1-\phi}{\phi} \qquad \text{equation 2-1}$$

Then, assuming that $Fe_2O_3$ is totally found as Fe(II)-rich biotite, i.e. annite, the abundance of annite is obtained as follows:

$$\frac{mol_{annite}}{L} = \frac{mol_{Fe}}{L} \cdot \frac{1\,mol_{annite}}{3\,mol_{Fe}} \qquad \text{equation 2-2}$$

Similar calculations can be performed to estimate the abundance of calcite (mol/L) as a function of fracture porosity.

**Table 2-2. Estimation of annite and calcite (both in mol/L) in a Forsmark fracture for two given porosities, and for the rock domain.**

| | | Fracture | | Rock | |
|---|---|---|---|---|---|
| Porosity ($\phi$) | | 0.1 | 0.2 | | 0.02 |
| $Fe(II)/Fe_{TOT}$ | | 1 | 1 | | |
| Annite | 2.5%wt $Fe_2O_3$ | 2.531 | 1.125 | 2%wt [1)] | 15.58 |
| | 17.5%wt $Fe_2O_3$ | 17.719 | 7.875 | | |
| Calcite | 14.4% | 35 | 15.52 | 0.4% | 5.4 |

[1)] 2%wt is the %Fe(II) in the rock.

Usually, dissolution rates of silicate and aluminosilicate minerals, R ($mol \cdot m^{-2} \cdot y^{-1}$), are written as a function of proton concentration by means of empirical rate laws:

$$R = k_H [H^+]^m + k_0 + k_{OH} [H^+]^n \qquad \text{equation 2-3}$$

which describes parallel acid- and base-promoted dissolution reactions. In equation 2-3, $k_H$, $k_0$ and $k_{OH}$ are respectively the acid, neutral and alkaline constants. The reaction orders, n and m, /Malmström and Banwart 1997, Lasaga 1995/ are normally fractional due to the existence of a variety of surface sites with different adsorption and reaction energies. In other words, reaction orders are a composite exponent indicating the speciation of the solid surface /Lasaga 1995/.

The kinetics of biotite dissolution has been studied by /Malmström et al. 1995/ as a function of pH. As in most aluminosilicate cases, the dissolution rate is pH dependent, showing a minimum around the $pH_{pzc}$ of the mineral. No data for the pure ferrous series end-member are available and, therefore, we have taken the rate law determined in the aforementioned work as representative of annite dissolution (see Figure 2-3):

$$R_{Fe} = 6.96.10^{-2}[H^+]^{0.51} + 5.28.10^{-11}[H^+]^{-0.65} \qquad \text{equation 2-4}$$

The rate of iron release, $R_{Fe}$, is assumed independent of the degree of undersaturation. But when the solution is oversaturated, no mineral dissolution occurs.

The set of minerals considered in the model is shown in Table 2-3.

A key parameter in kinetic calculations is the surface area of the mineral available for reaction (A in $m^2/g$). However, it is hard to find a given value which is robust and reliable, besides the notable contributions of /Malmström et al. 1995/. More recent data on surface area of biotite /Samson et al. 2005/ were obtained for the 53 to 105 µm size fraction. The surface areas are 3.6 and 3.65 $m^2/g$ respectively, whereas /Malmström et al. 1995/ obtained 1.81 $m^2/g$ for the 75 to 125 µm size fraction. Release rate normalised to the mineral stoichiometry and surface area obtained by /Samson et al. 2005/ are very consistent with those of /Malmström and Banwart 1997/ for pH values below 9, while for pH above 10 dissolution rates in Malmström and Banwart are slightly higher than those in /Samson et al. 2005/. This probably indicates precipitation problems at high pH values in the later reference, as highlighted by those authors in their result discussion.

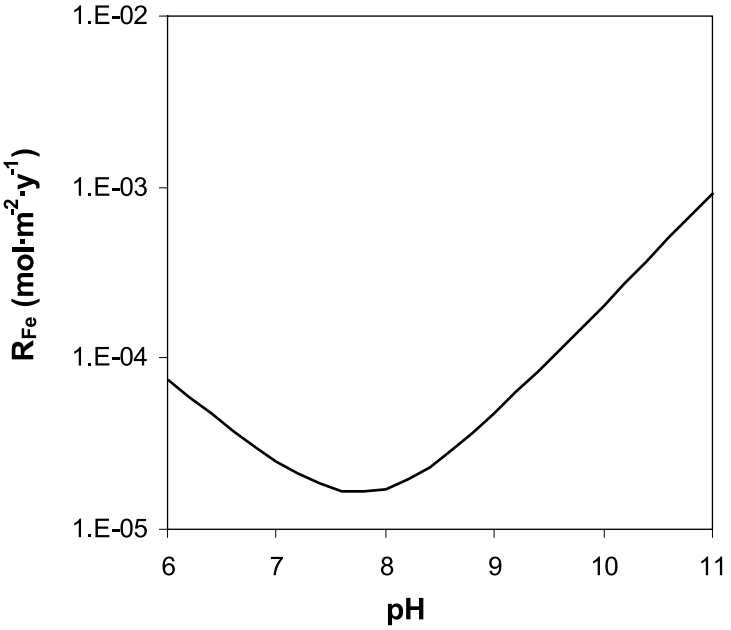


***Figure 2-3.*** *The rate of Fe(II) release from biotite dissolution from /Malmström et al. 1995/ as a function of pH.*

**Table 2-3. Set of minerals considered in the model. Dissolution of minerals at equilibrium is controlled by the solubility product.**

| Minerals | Reaction | |
|---|---|---|
| **Primary minerals** | | |
| Fe-Biotite (Annite) | $KFe_3AlSi_3O_{10}(OH)_2 + 10\ H_2O = K^+ + 3Fe^{2+} + Al(OH)_4^- + 3H_4SiO_4 + 6OH^-$<br>$R_{Fe}$ (mol·m$^{-2}$·y$^{-1}$) = $6.96\cdot10^{-2}[H^+]^{0.51} + 5.28\cdot10^{-11}[H^+]^{-0.65}$ /Malmström et al. 1995/ | equation 2-5 |
| Calcite | $CaCO_3 = CO_3^{2-} + Ca^{2+}$<br>log $K_{eq}$ = –8.480 /Hummel et al. 2002/ | equation 2-6 |
| **Secondary minerals** | | |
| Chalcedony | $SiO_2 + 2H_2O = H_4SiO_4$<br>log $K_{eq}$ = –3.55 | equation 2-7 |
| Kaolinite | $Al_2Si_2O_5(OH)_4 + 6H^+ = 2Al^{3+} + 2H_4SiO_4 + H_2O$<br>log $K_{eq}$ = 7.435 | equation 2-8 |
| Hematite | $Fe_2O_3 + 6H^+ = 2Fe^{3+} + 3H_2O$<br>log $K_{eq}$ = –4.008 | equation 2-9 |
| $Fe(OH)_3$(a) | $Fe(OH)_3 + 3\ H^+ = Fe^{3+} + 3\ H_2O$<br>log $K_{eq}$ = 5.656 /Johnson 2000/ | equation 2-9 |
| Dolomite | $CaMg(CO_3)_2 = Ca^{2+} + Mg^{2+} + 2CO_3^{2-}$<br>log $K_{eq}$ = –17.09 | equation 2-10 |

Although the most recent data from /Samson et al. 2005/ had not appeared at the time when the calculations were conducted within this project were in progress, the consistence between the different sources of data in the literature give additional confidence to the parameters selected for this analyses.

We have proceeded in this work similarly to previous works /Guimerà et al. 1999/ and have minimised the impact of the uncertainty associated to the surface area of the solid on the results by conducted a sensitivity analysis (see following Chapters 3 and 4).

In this report the surface area available for reaction per volume of groundwater, $S_A$ (m$^2$/L), is estimated as follows:

$$S_A = A \cdot MM_{\text{mineral}} \cdot \frac{mol_{\text{mineral}}}{L} \qquad \text{equation 2-11}$$

A is uncertain, because it depends on the particle diameter. We assume that $A_{annite}$ is 1.81 m$^2$/g for size fractions between 75 and 125 μm /Malmström et al. 1995/ although the obtained value is for biotite. In equation 2-11, we use for annite an average value of 1.5 m$^2$/g, a molecular mass of 511.88 g/mol and an initial concentration in the fracture of 1.125 mol/L (see Table 2-2). The resultant $S_A$ is 864 m$^2$/L. Given the large uncertainty of this parameter, we arbitrarily assign to it a value 100 times lower (8.64 m$^2$/L) accounting for a lower accessibility of the surface area in the media. Notice that in our model $S_A$ is constant and annite dissolution (equation 2-4 ) is therefore independent of variations in $S_A$, which may be a major simplification of our model.

### 2.2.2 Groundwater composition data

The composition of the reference Forsmark deep groundwater /SKB 2004/ is detailed in Table 2-4. It corresponds to the groundwater sampled in Forsmark on the 13$^{th}$ of June 2003 packed in the interval 509–516.08 m from borehole KFM02A (SICADA database, /SKB 2004/).

Forsmark deep groundwater is considered as the water flowing through the fractures. Reactions as dissolution or precipitation of secondary minerals such as chalcedony, kaolinite and ferric hydroxide as $Fe(OH)_3$(am) or hematite are considered fast reactions, that rapidly achieved equilibrium. As a consequence, the initial composition of the Forsmark water changes slightly during the first time step of the model calculations as it becomes equilibrated with these minerals. The initial water is then undersaturated with Fe(II) aluminosilicates such as chlorite. The compositions are detailed in Table 2-4 and compared with the waters used in /Guimerà et al. 1999/ in Table 2-5.

**Table 2-4. Selected composition (M) of initial water in fractures and intrusive water in the domain as equilibrated ice melting water.**

| Components | Forsmark groundwater | Initial water in fractures [1)] | Grimsel groundwater [2)] | Equilibrated ice melting water [3)] |
|---|---|---|---|---|
| pH (–) | 7.0 | 6.95 | 9.6 | 6 |
| Eh (mV) | –143 | –189 | –200 | 864 |
| $[Na^+]_{tot}$ | $8.88\cdot10^{-02}$ | $8.88\cdot10^{-02}$ | $6.90\cdot10^{-04}$ | $6.90\cdot10^{-04}$ |
| $[K^+]_{tot}$ | $8.75\cdot10^{-04}$ | $8.75\cdot10^{-04}$ | $5.00\cdot10^{-06}$ | $5.00\cdot10^{-06}$ |
| $[Ca^{2+}]_{tot}$ | $2.33\cdot10^{-02}$ | $2.33\cdot10^{-02}$ | $1.40\cdot10^{-04}$ | $1.40\cdot10^{-04}$ |
| $[Mg^{2+}]_{tot}$ | $9.30\cdot10^{-03}$ | $9.30\cdot10^{-03}$ | $6.20\cdot10^{-07}$ | $6.20\cdot10^{-07}$ |
| $[HCO_3^-]$ | $1.77\cdot10^{-03}$ | $2.03\cdot10^{-03}$ | $4.50\cdot10^{-04}$ | $1.57\cdot10^{-05}$ |
| $[Cl^-]_{tot}$ | $1.53\cdot10^{-01}$ | $1.53\cdot10^{-01}$ | $1.60\cdot10^{-04}$ | $4.04\cdot10^{-04}$ |
| $[S]_{tot}$ | $6.80\cdot10^{-03}$ | $6.80\cdot10^{-03}$ | $6.10\cdot10^{-05}$ | $6.10\cdot10^{-05}$ |
| $[Br^-]_{tot}$ | $2.98\cdot10^{-04}$ | $2.98\cdot10^{-04}$ | $3.80\cdot10^{-07}$ | $3.80\cdot10^{-07}$ |
| $[Si]_{tot}$ | $1.85\cdot10^{-04}$ | $2.67\cdot10^{-04}$ | $2.50\cdot10^{-04}$ | $2.50\cdot10^{-04}$ |
| $[Fe]_{tot}$ | $3.31\cdot10^{-05}$ | $1.00\cdot10^{-06}$ | $3.00\cdot10^{-09}$ | $3.00\cdot10^{-09}$ |

[1)] Groundwater composition obtained in the fracture after the first time step of the simulations, as a result of equilibrating the "Forsmark groundwater" with fracture minerals (calcite, chalcedony, kaolinite and haematite).

[2)] Grimsel groundwater composition, discharging groundwater from the Migration shear zone [AU 96]. Data compiled from /Bajo et al. 1989, Aksoyoglu et al. 1990/ and /Eikenberg et al. 1991/.

[3)] Grimsel groundwater equilibrated with atmospheric $O_2$ and $CO_2$. $[O_2] = 2.74\cdot10^{-4}$M (i.e. 8.76 mg/L).

**Table 2-5. Comparison with /Guimerà et al. 1999/ of initial and ice melting waters.**

| Components | Initial water (this study) | Initial water /Guimerà et al. 1999/ | Ice melting water (this study) | Ice melting water /Guimerà et al. 1999/ |
|---|---|---|---|---|
| pH | 6.95 | 7.7 | 6 | 8.15 |
| Eh (mV) | –143 | –118 | 864 | 710 |
| $C_{tot}$(M) | $1.983\cdot10^{-3}$ | $0.164\cdot10^{-3}$ | | |

No clear agreement on the composition of typical ice melting water is available in the literature. In the previous work of /Guimerà et al. 1999/, the composition of the water reported by /Yang et al. 1996/ equilibrated with Fe(III) hydroxide, calcite and high concentration of oxygen was used for this purpose.

In this stage of the project, we have used a slightly different composition. The composition of the Grimsel groundwater has been considered as representing the result of the interaction of ice melting water with granitic minerals. This water presents a very low ionic strength, as expected from a very diluted water infiltrating and interacting at relatively fast velocities through a granitic fracture.

From a conceptual point of view, it is expected that waters from ice melting interact with some fracture filling minerals before contacting the reducing zone. Therefore, we have assumed that waters from ice melting have the composition of the Migration shear zone of Grimsel [AU 96] after interaction with atmospheric oxygen and $CO_2$. The Grimsel composition corresponds to that reported in /Bajo et al. 1989, Aksoyoglu et al. 1991/ and /Eikenberg et al. 1991/ (see Table 2-4). After equilibration with atmospheric $O_2$(g) ($P_{O_2} = 0.2$ atm) and $CO_2$(g) ($P_{CO_2} = 10^{-3.5}$ atm), the changes in the composition of the Grimsel groundwater affect mainly to pH and redox potential (see Table 2-4).

As can be observed in Table 2-5, the initial and intrusive waters selected in this project are slightly less alkaline than in /Guimerà et al. 1999/.

## 2.3 Hydrodynamics

### 2.3.1 Generalities

It is far beyond the scope of this report to gain insight or to present a thorough review of the recent conceptual understanding of groundwater flow and solute transport in low permeability fractured media. Over the past decade, fundamental papers and books have been published summarising the key findings of two worldwide issues: the selection of repository sites for radioactive waste isolation and groundwater pollution in fractured rocks /Bodin et al. 2003/. Among the reviews of general interest are: /Bear et al. 1993, Sahimi 1995ab, NRC 1996, Adler and Thovert 1999, Fabishenko et al. 2000/ and /Bodin et al. 2003/. Specific issues on solute transport are treated by /Williams 1996/ and non saturated issues by /Pruess et al. 1999/ and /Fabishenko et al. 2000/ as well.

In fact, calculations made in this report will concentrate in the geochemical changes that occur in a reduced part of a system of concern for a repository, such as one single fracture or a host rock where water flows as in a continuum medium.

Following we explain how these models are used in this project.

### 2.3.2 Single porosity system

A single porosity system is used to describe the geochemical changes in both the single fracture and the host rock. The geochemical changes in this system will be calculated by means of the PHREEQC code /Parkhust and Appelo 1999/. As explained in Chapter 3, this code calculates equilibrium and kinetic reactions in cells. Each cell contains a litre of water and a number and amount of solid minerals defined by the user. A given domain can be simulated by a number of cells, and the user can define that the water in one cell replaces the water in the following one at a given rate. Cells are given a certain length which permits to define the dimension of the problem with the proper number of cells. Needless to say that the problem is always envisaged in one dimension. The rate at which the water replacements are made provides the time dimension of the problem. Hence, one can make the geochemical calculations, imposing that water is flowing at a given "velocity" in the domain. Calculations are run for a given simulation time, which is also defined by the user. Further details on the numerical algorithms of the code can be found in the user's guide /Parkhust and Appelo 1999/.

For this type of calculations, the classical hydrodynamic parameters must be adapted to the needs of the code. For instance, no hydraulic conductivity, transmissivity or fracture thickness is used, and the same applies for the hydraulic gradient. Porosity is only used to define the mineral content in Table 2-2. Therefore, the rate at which the water replacements take place and the number and dimensions of the cells are accommodated to honour a certain groundwater velocity. As we will discuss later, this velocity will be set to $10^{-7}$ and $10^{-9}$ m/s for the base cases in the fracture and rock domains, respectively.

## 2.4 Definition of the base cases

The conceptual model consists in the intrusion of oxygenated groundwater into the domain. The source of oxygen is depleted by Fe(II) released from annite dissolution. The main minerals present in the system (calcite, kaolinite and chalcedony) control by equilibrium the consequent changes in pH, aluminium and silica contents respectively. The rate of Fe(II) supply is kinetically controlled by the dissolution of annite. Therefore, the oxidant front moves downstream if either the reducing capacity is consumed or annite dissolution does not supply fast enough Fe(II). Flow velocity and annite abundance are determinant of oxidant front advancement.

According to the hydrogeochemical models discussed before, two different base cases deserve special analysis and will be considered for calculation with numerical models: fracture system and fractured rock system. They mainly differ on flow velocity and mineral content. They are summarised in Table 2-6.

The first base case (1 in Table 2-6) represents the shortest flowpath to the repository, as a 400 m long homogeneous fracture. Forsmark water equilibrated with secondary minerals is present initially in the whole domain (Table 2-4). Calcite and annite distribution is homogeneous all over the domain. The ice melting water equilibrated with $O_2(g)$ and $CO_2(g)$ enters by the top boundary of the domain.

Despite the fact the results of numerical calculations on the hydrodynamic conditions during the periods of deglaciation estimate the maximum groundwater velocity to $1.6 \cdot 10^{-9}$ m/s for infiltrating meltwater /Svensson 1999, Jaquet 2006/ a more conservative value is selected for the fracture base case (1, see Table 2-6). The groundwater velocity is $1 \cdot 10^{-7}$ m/s, two orders of magnitude above the one predicted. Also the fracture porosity of 0.2 and a Fe content of 2%wt $Fe_2O_3$ are considered, (Table 2-2).

The second base case (2 in Table 2-6) represents the whole block of granite as a homogeneous porous media. In this model, the characteristics of the rock matrix are taken into account. The main differences with the fracture system case are a lower groundwater velocity ($1 \cdot 10^{-9}$ m/s), a lower equivalent porosity (0.02) and a lower content of biotite and calcite as indicated in Table 2-1, Table 2-2 and Table 2-6. Figure 2-4 shows how we envisage the conceptual model and the way it will be implemented in a numerical model, which is explained in Chapter 3. Recall that both, these two base cases are essentially the same in terms of domain and boundary conditions; therefore, the same figure applies to both.

Table 2-7 compares the parameter values used in /Guimerà et al. 1999/ with the current values used in the single porosity models of this project.

**Table 2-6. Hydraulic and geochemical set of parameters for the three conceptual models: the fracture and host rock model.**

| Model | 1. Fracture | 2. Host rock |
|---|---|---|
| v (m/s) | $1 \cdot 10^{-7}$ | $1 \cdot 10^{-9}$ |
| K (m/s) | $2 \cdot 10^{-7}$ [1)] | $2 \cdot 10^{-10}$ [1)] |
| $\phi$ (–) | 0.2 [1)] | 0.02 [1)] |
| $\nabla H$ (–) | 0.1 [1)] | 0.1 [1)] |
| Annite abundance (mol/L) | 1.125 | 15.58 |
| Annite $S_A$ ($m^2$/L) [2)] | 8.64 | $8.64 \cdot 10^{-2}$ |
| Calcite abundance (mol/L) | 15.5 | 5.4 |

[1)] Calculations will be made with a code that only makes use of groundwater velocity, but this parameter is presented as indicative of the case.

[2)] Recall that the conversion from $m^2$/g to $m^2$/L is given by equation 2-11.

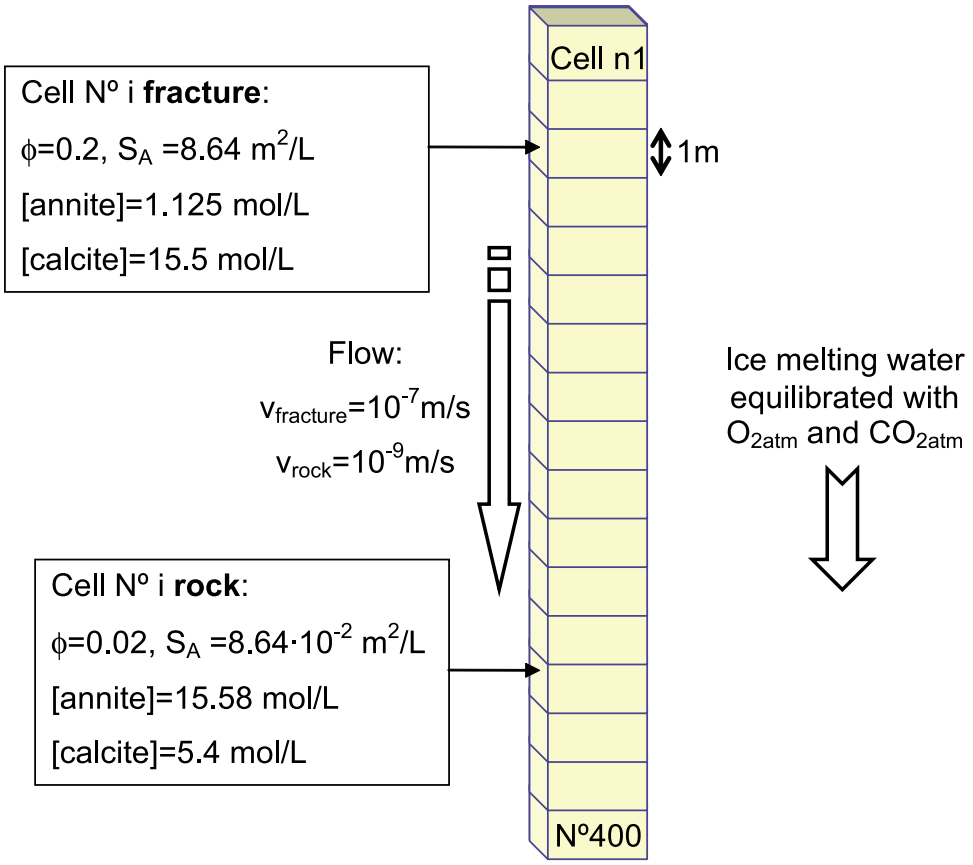


***Figure 2-4.*** *Numerical model for the base cases of the 1D systems (fracture or rock) and the initial conditions.*

**Table 2-7. Set of parameters used for the calculations of single porosity models and comparison with former values used by /Guimerà et al. 1999/.**

| | Present study | | Parameters used in /Guimerà et al. 1999/ | |
|---|---|---|---|---|
| | Fracture | Host rock | Fracture | Host rock |
| K (m/s) | $2\cdot10^{-7}$ [1)] | $2\cdot10^{-10}$ [1)] | $10^{-7}$ | $10^{-9}$ |
| ϕ (–) | $2\cdot10^{-1}$ [1)] | $2\cdot10^{-2}$ [1)] | $10^{-2}$ | $10^{-3}$ |
| v (m/s) | $10^{-7}$ | $10^{-9}$ | $10^{-6}$ | $10^{-10}$ |
| ∇H (–) | $1\cdot10^{-1}$ [1)] | $1\cdot10^{-1}$ [1)] | $1\cdot10^{-1}$ | $1\cdot10^{-1}$ |
| Mineral abundance (mole/L) | 1.125 (annite) | 15.58 (annite) | 91.8 (chlorite) | 447 (biotite) |

[1)] Parameters not directly implemented into the code but indicative of the case.

# 3 Numerical models

This chapter presents the methodology used to solve numerically the conceptual models presented previously.

PHREEQC v2.10 /Parkhurst and Appelo 1999/ has been used to solve the two systems previously cited in Chapter 2. The numerical structure is described. A sensitivity analysis on numerical parameters of the model has been performed in order to optimize the convergence of the problem and to minimize the numerical errors. Finally the selected numerical models for each system are described.

## 3.1 Codes

Single porosity simulations for the fracture and rock systems are performed with PHREEQC v2.10 /Parkhurst and Appelo 1999/. PHREEQC is a computer code for simulating chemical reactions and transport processes in natural or polluted groundwaters that is based on equilibrium chemistry of aqueous solutions interacting with minerals, gases, solid solutions, ion exchangers and sorption surfaces. It also includes the capability to model kinetic reactions with rate equations specified by the users. Moreover, it includes an explicit finite difference algorithm for calculations of 1-D advective-dispersive transport and optionally, diffusion in stagnant zones.

The domain is discretized into a given number of cells, and the transport is simulated by consecutive replacement of the pore water contained in one cell. Each cell is assumed to contain one litre of pore water. The water initially filling cell n°1 is transported to cell n°2 and subsequently with each shift or water replacement. The water velocity is given by the time step associated with each shift or water replacement.

## 3.2 Structure of the models

Our model represents a 400 m long homogeneous medium, which is either a fracture system or a rock system. It is composed by 400 homogeneous cells. Hence, amount of calcite and annite is homogeneously distributed all over the domain and the mineral content depends on the case considered. Forsmark water equilibrated with secondary minerals is initially present in the system. The ice melting water equilibrated with $O_2(g)$ and $CO_2(g)$ enters by the top boundary of the domain as explained in Chapter 2. Figure 2-4 represents a schematic view of the system, with the initial conditions either for the fracture system or the equivalent rock system. Note that both systems are numerically identical in terms of space and time discretization. Section 2.4 indicates the reference parameters and variables for both.

As regards discretization, the choice of the longitudinal discretization is critical for the numerical stability of the model. Table 3-1 shows the parameters proposed for distances of 400 m. Single porosity and coarse grids are selected, and the simulation time is comparable to the deglaciation period (5,000 years). A space discretization of 1 m and a time discretization of 27.4 days ensure results that are stable, accurate enough and the solution will last approximately 1 day.

**Table 3-1. Selection of some parameters to optimize the numerical calculations.**

| | v (m/s) | Length (m) | $\Delta x$ (m) | $t_{sim}$ (y) | $\Delta t$ (s) | Pe | CPU (days) |
|---|---|---|---|---|---|---|---|
| 1D model | $10^{-7}$ | 400 | 1 | 5,000 | $10^7$ | 1 | 1 |

CPU = computational time

As pointed out in the previous section, a critical parameter is the content of annite in the fracture. At a given time, the abundance of mineral is calculated as:

$$\left[\frac{mol_{annite}}{L}\right]^{t} = \left[\frac{mol_{annite}}{L}\right]^{t-1} - R_{Fe}^{t} \cdot S_{A} \cdot \Delta t \qquad \text{equation 3-1}$$

The last term of equation 3-1 stands for annite depletion during one time step (Δt), which depends on the dissolution rate (equation 2-4) and the surface area (equation 2-11). To sum up, the annite content in the domain, therefore the depletion of oxygen depends on:

- The initial content of annite (mol/L), which is in function of domain porosity.
- The release of Fe(II), implemented in the code as the kinetic law described in equation 2-4, which depends on the variation of pH and annite saturation degree (see Appendix).
- $S_A$ ($m^2$/L) proportional to the domain porosity.

# 4 Results

This chapter reports the results of the simulations. The core of the analyses is the evolution of the dissolved oxygen in the system and the associated changes on: annite presence (by dissolution), redox potential, precipitation of Fe(III) forms, calcium concentration, calcite presence, and pH. The simulations have been extended to a maximum time length of 5,000 years, equivalent to a de-glaciation episode. It is worth to remember that the depth 400 m corresponds to the repository depth. All the hydrodynamics and geochemical parameters selected for each base case are summarized in Chapters 2 and 3.

## 4.1 Fracture system

In this system, the study is first described over 100 years in order to understand the basic processes. Then, the evolution over a de-glaciation period of 5,000 years is discussed.

The groundwater velocity of the base case in the fracture media is $10^{-7}$ m/s (Table 2-7) and the conservative tracer (bromide) reaches the repository depth in 130 years. As observed in Figure 4-1, the concentration of bromide in the system equals the concentration of the ice-melting water after 100 years at a depth of 300 m, in agreement with the groundwater velocity.

The advance of the calcium depletion is plotted in Figure 4-1 at 10, 60 and 100 years after the infiltration proceeds and is similar as bromide.

The pH of the ice melting water is given by equilibrium with atmospheric $CO_2$. When this type of water contacts calcite present in the media, the solid dissolves in order to reach equilibrium, what causes an increase of pH up to 9.8 (Figure 4-2).

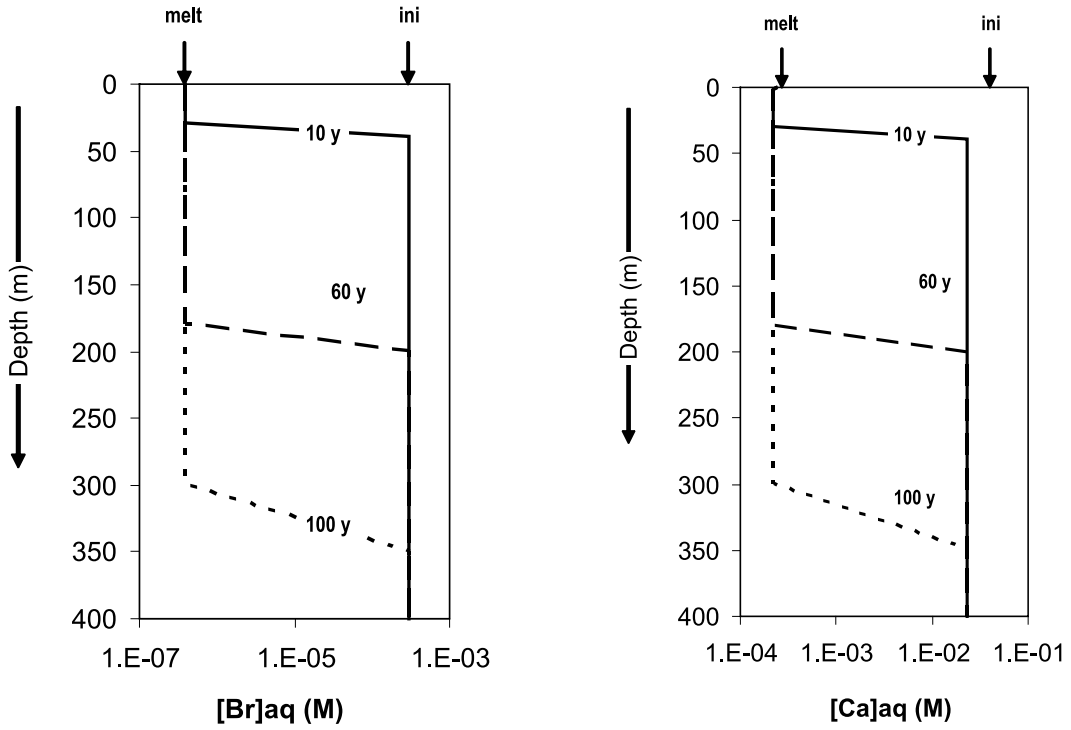


***Figure 4-1.*** *Evolution of the aqueous bromide and calcium concentration along the flowpath in the base case of the fracture system over 100 years. "Ini" is the initial water concentration value and melt the value of the intrusive water.*

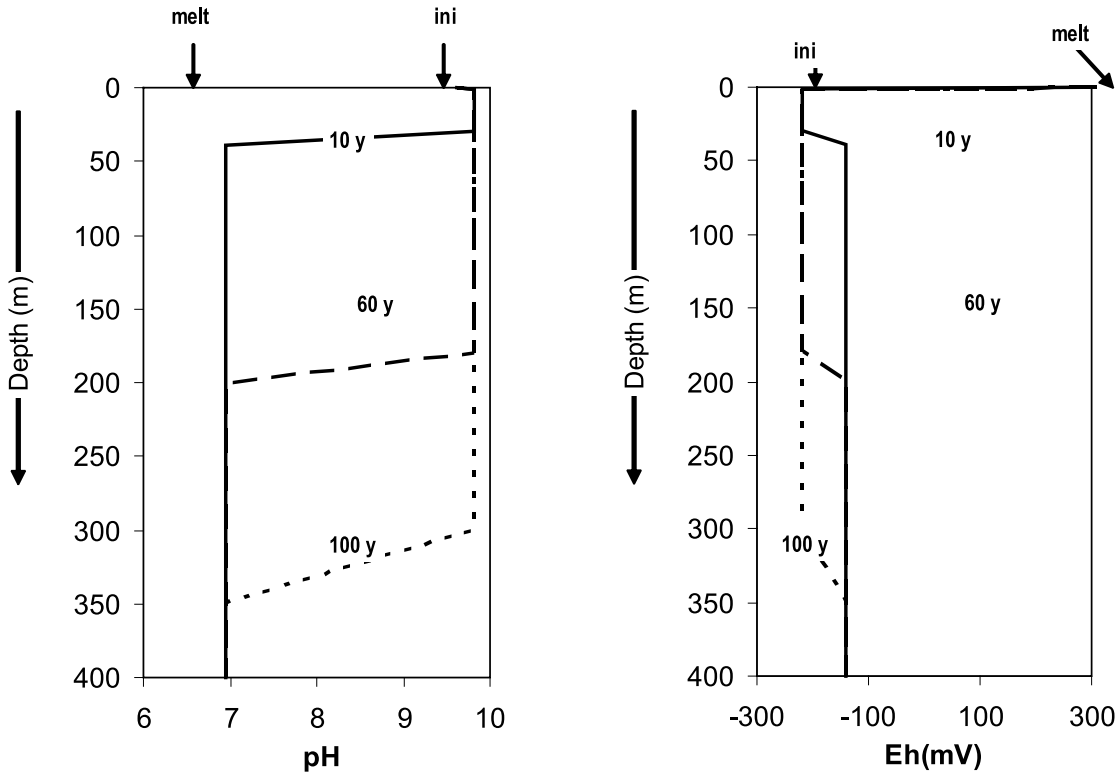


***Figure 4-2.*** *Evolution of the pH and redox potential along the flowpath in the base case of the fracture system over 100 years. "Ini" is the initial water concentration value and melt the value of the intrusive water. Recall that the redox potential of melt water is set at 864 mV or pe approx 14 (Table 2-4).*

This equilibrium pH is very similar to the one of the original Grimsel groundwater prior to its equilibrium with atmospheric $CO_2$ and $O_2$ (see Table 2-4). pH does never reach values as low as the initial melt water, given that it is a closed system, where $P_{CO_2}$ is not fixed and therefore, equilibrium with calcite will control the pH of the groundwater.

In the same Figure 4-2 the evolution of the redox potential is shown. The system, initially at a Eh = −189 mV (according to Table 2-4), is able to buffer the oxidant intrusion by means of oxidation of the Fe(II) released from annite. Once glacial melt water infiltrates, the final redox potential reached in the system is slightly lower than the initial one due to the equilibrium established in the system with $Fe(OH)_3$(am) at a higher pH. Figure 4-3 shows the evolution of the master variables pH and redox potential in a Pourbaix diagram of the iron system.

The oxygen content in ice melting water is $2.74 \cdot 10^{-4}$ mol/L (see Table 2-4) due to the equilibrium with atmospheric $P_{O_2}$ (g). All oxygen is consumed by Fe(II) released by the dissolution of annite. After 100 years the front of annite dissolution progresses a maximum of 2.5 metres depth, which has caused the precipitation of $Fe(OH)_3$(am) (Figure 4-4).

As a consequence of the dissolution of annite, Fe(II) is released and oxidized by the dissolved oxygen into Fe(III), and this precipitates as $Fe(OH)_3$(am). The concentration of iron in solution is, then, given by the equilibrium with $Fe(OH)_3$(am), as it is shown in Figure 4-5.

When the system is studied over a de-glaciation period of 5,000 years, the evolution of pH, redox potential and oxygen is slightly different. The oxygen advance front is directly related to the depletion of annite in the system (see Figure 4-6).

Ⓐ Infiltrating GW
Ⓑ Initial GW in fractures

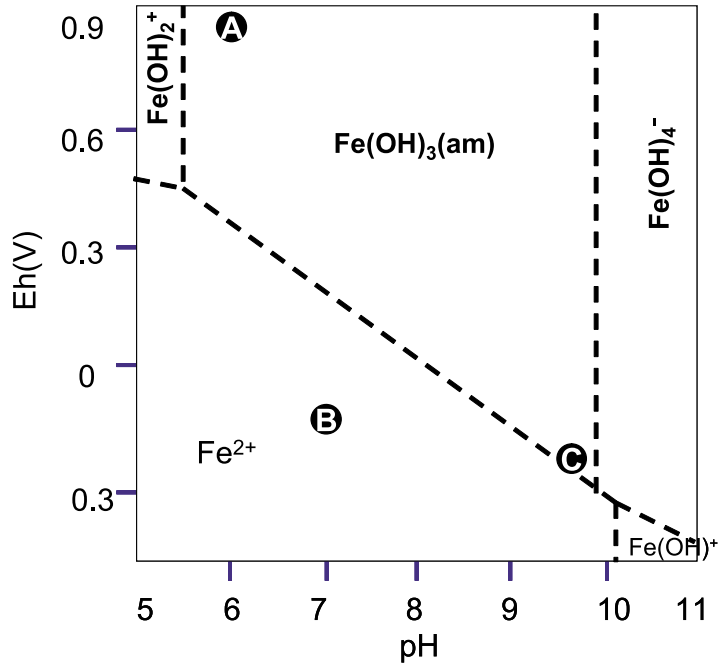


***Figure 4-3.*** *Eh-pH diagram of the system. A indicates the initial value of the master parameters in the infiltrating groundwater; B stands for the initial water in fractures. C indicates the final state of the water after the infiltration of the melting groundwater, what results in an increase of pH buffered by calcite dissolution and a decrease of the redox potential due to Fe(II) oxidation.*

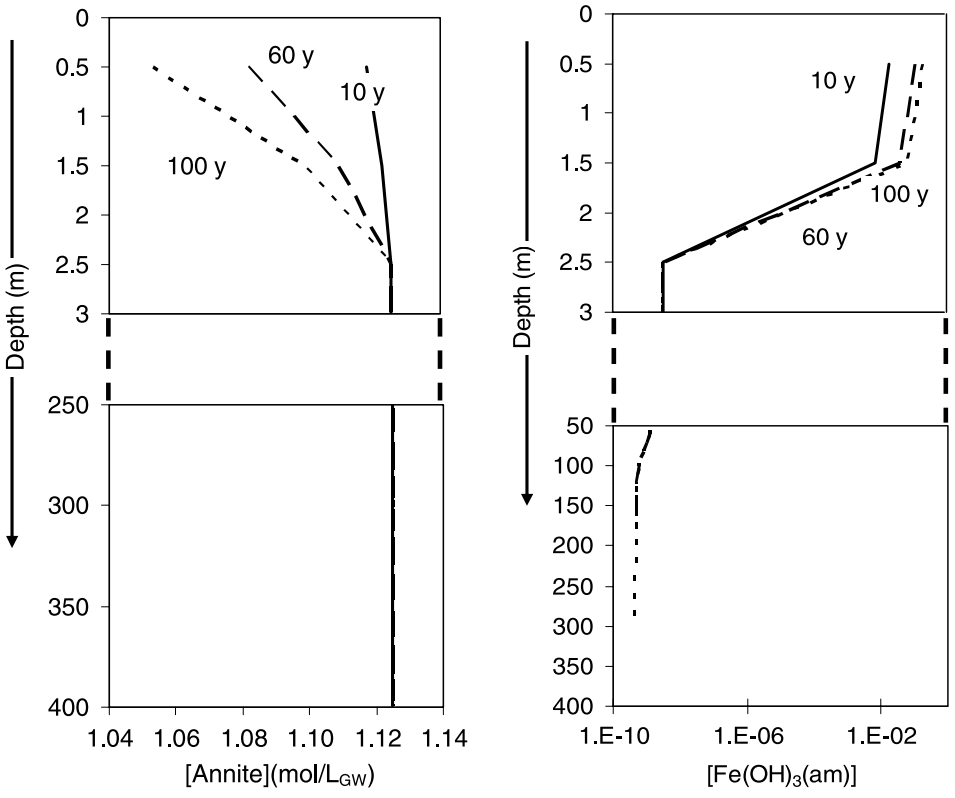


***Figure 4-4.*** *Evolution of the content of annite and precipitated $Fe(OH)_3(am)$ with depth in the base case of the fracture system over 100 years.*

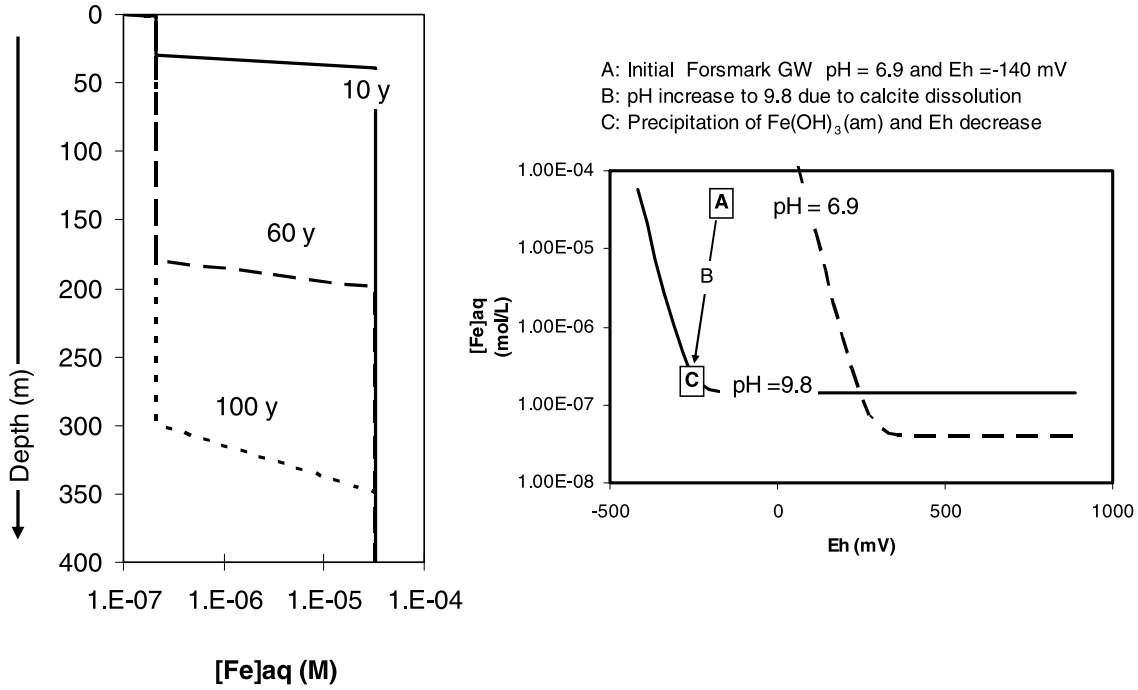


***Figure 4-5.*** *Evolution of the content of total aqueous iron along the flowpath in the base case of the fracture system over 100 years and limitation by the solubility of $Fe(OH)_3(am)$.*

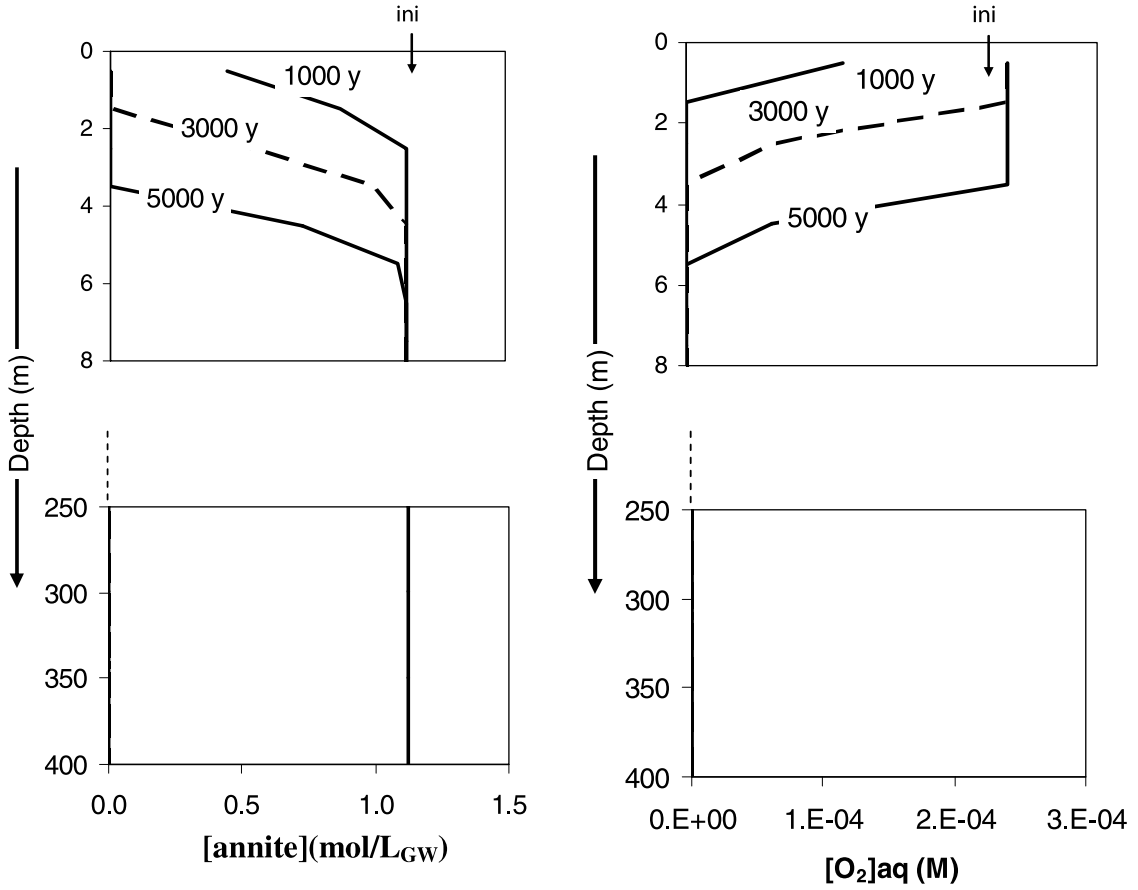


***Figure 4-6.*** *Evolution of the content of annite and dissolved oxygen along the flowpath in the base case of the fracture system over 5,000 years. "Ini" stands for the initial water concentration value.*

The rate of annite depletion can be observed in Figure 4-7 in the first metres of the domain. One can appreciate that once annite is totally exhausted, the rate of annite dissolution in the cell located downflow increases, which is due to the fact that the inflowing water is not modified in the previous cell with regard to oxygen content.

Consequently, the oxygen remaining in the system is completely consumed, as indicated before. Figure 4-8 shows that indeed, no oxygen reaches the repository altitude for the simulation period.

The precipitation of secondary phases, such as kaolinite, $Fe(OH)_3(am)$, and chalcedony, which reflects the dissolved annite, is shown in Figure 4-9. The, formation of these solid phases keep the concentrations of aqueous Al and Fe on their corresponding solubility levels.

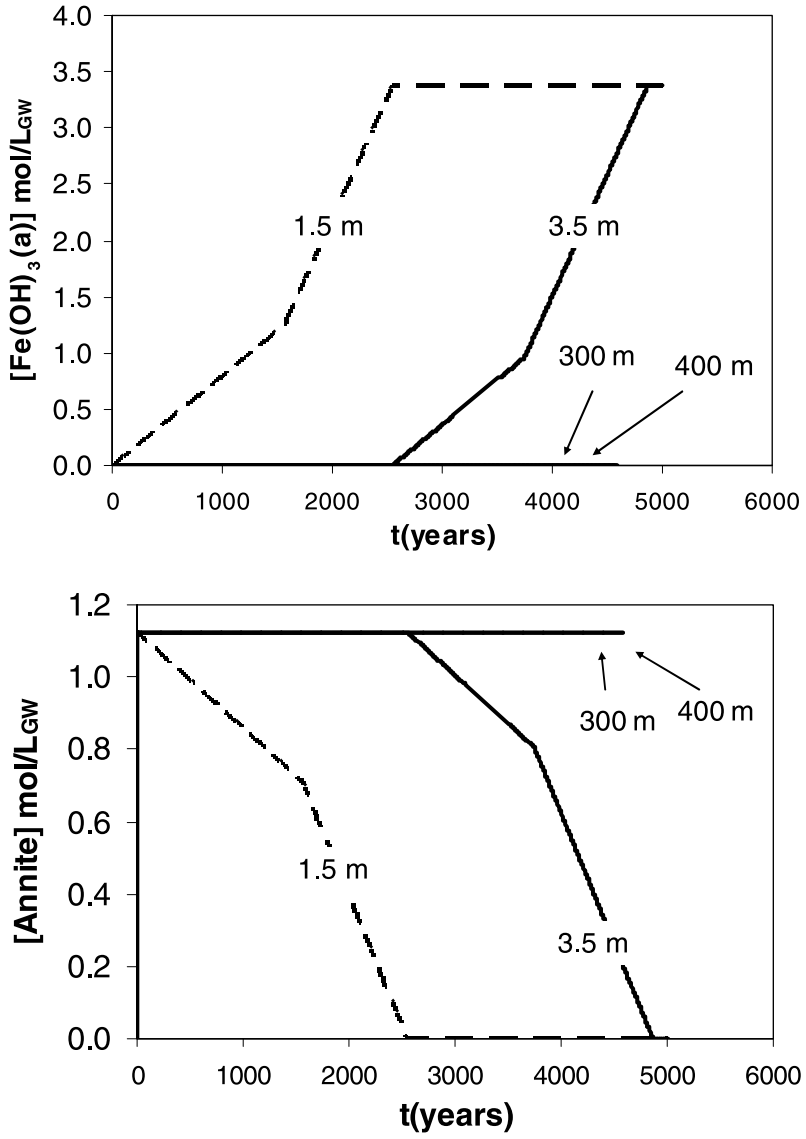


***Figure 4-7.*** *Evolution of the moles of annite remaining in the domain with time and precipitated $Fe(OH)_3(am)$ for different depths.*

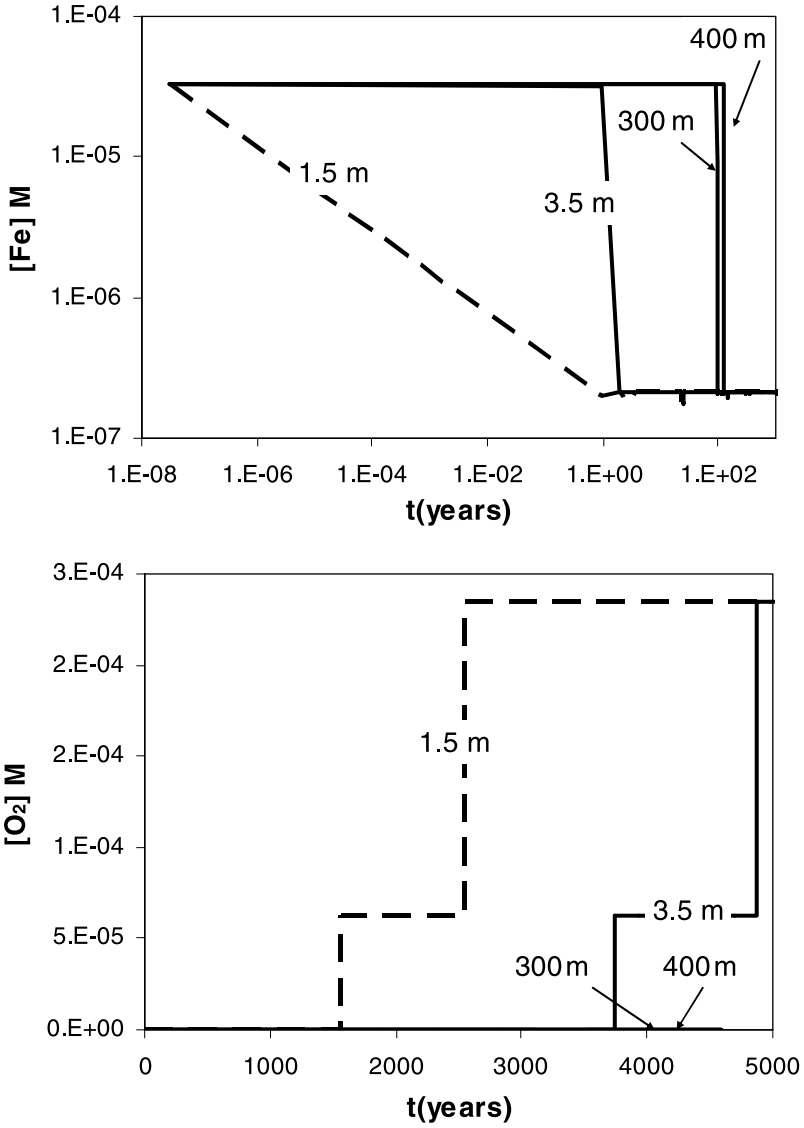


***Figure 4-8.*** *Oxygen content and iron in solution for the base case. Note that 400 m is the repository depth.*

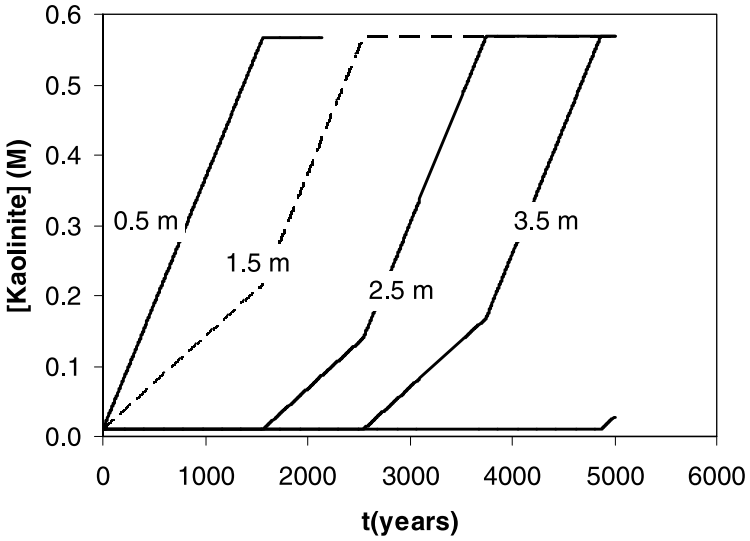


a) Kaolinite precipitation

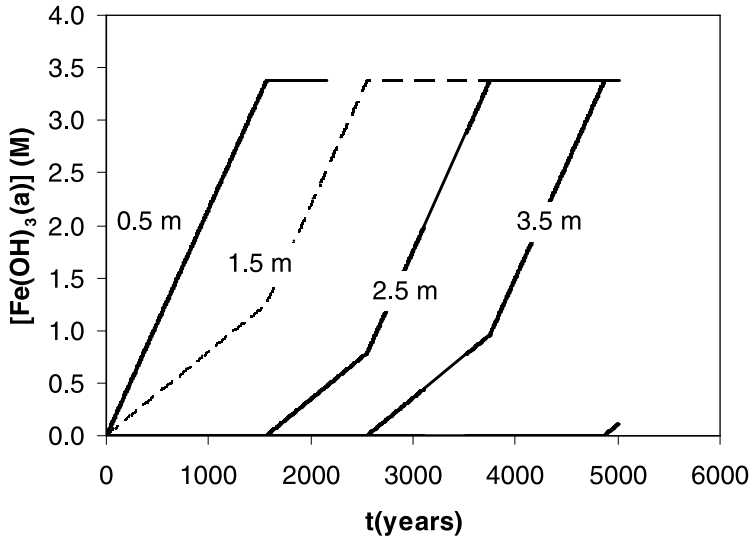


b) $Fe(OH)_3(am)$ precipitation

***Figure 4-9.*** *(1) Evolution of the moles of secondary minerals precipitating in the domain with time, for different depths.*

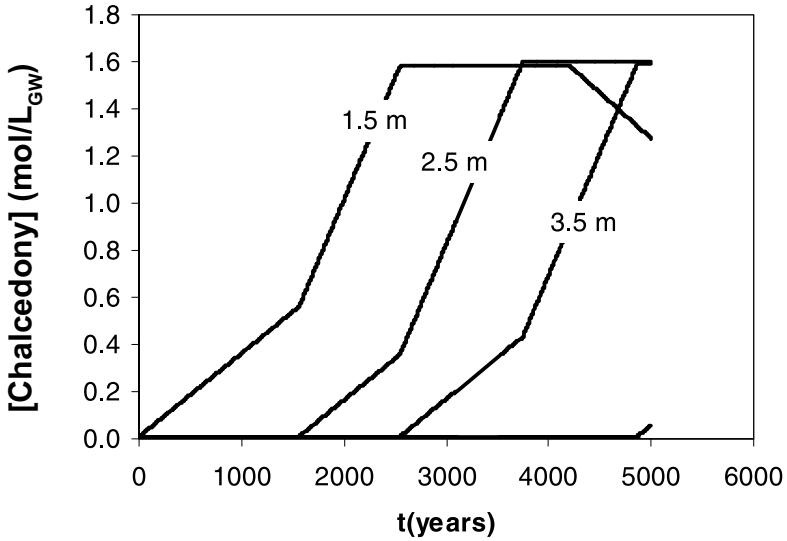


c) Chalcedony precipitation

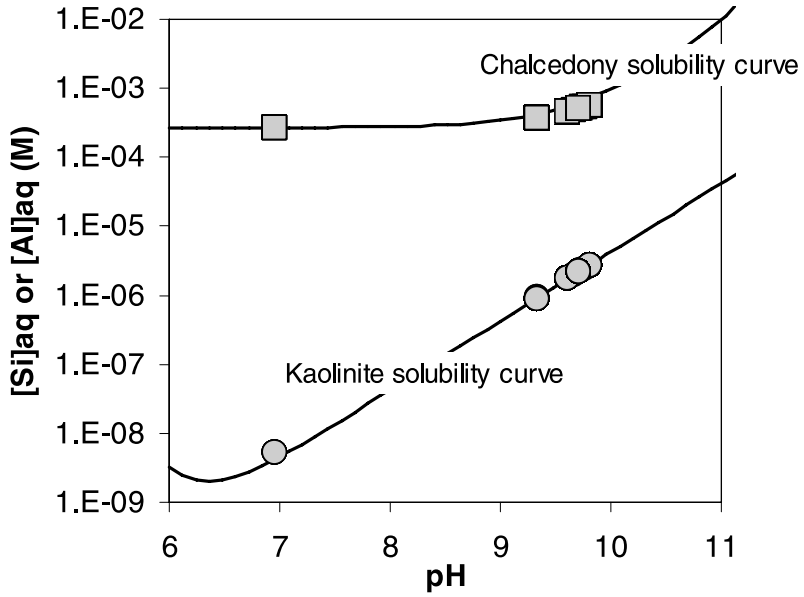


d) Si and Al concentrations in solution

***Figure 4-9.*** *(2) Evolution of the moles of secondary minerals precipitating in the domain with time, for different depths. d) Concentrations of aqueous Si and Al of the base case (symbols) compared with the solubility curves of chalcedony and kaolinite (lines). The solubility curves are calculated with the HYDRA-MEDUSA code package /Puigdomènech 2004/.*

The evolution of the master variables, pH and redox potential, is shown in Figure 4-10. According to the results obtained, it is not foreseen that the oxydising front reaches the repository depths over a deglaciation period. Oxygen is exhausted after several metres of domain and the oxidant front, according to the conceptual model implemented, is buffered by the dissolution of annite present in the fracture. Annite is depleted in the first metres of the system. As a consequence, the oxidant front reaches only 6 m deep after a 5,000 years of de-glaciation and oxygen is completely consumed.

### 4.1.1 Sensitivity analysis

As indicated in Chapters 2 and 3, some parameters are uncertain, while others display a wide range of variability. The way of dealing with this variability with 1D models is through sensitivity analyses. We have performed analyses on the hydrodynamic parameters and on geochemical variables. Table 4-1 compiles the parameters and their values used in the code for each case studied.

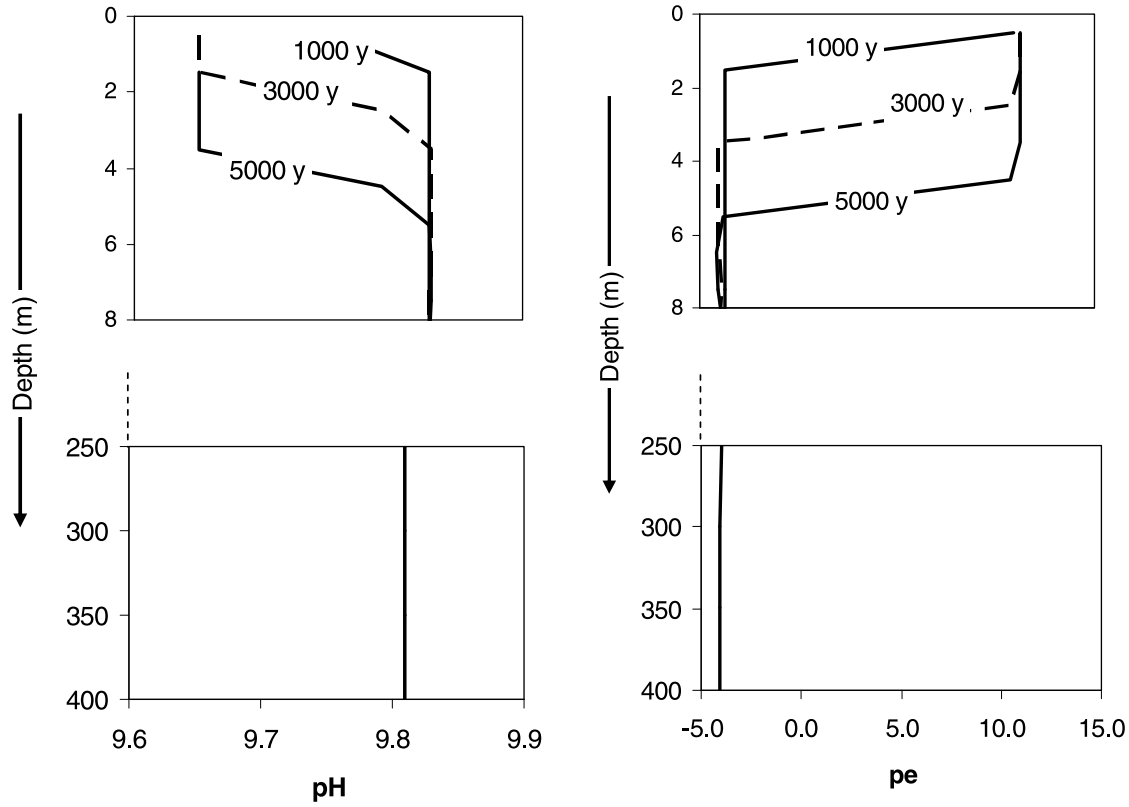


***Figure 4-10.*** *Evolution of the pH and redox potential (in terms of pe = Eh(mV)/59.16) along the flow-path in the base case of the fracture system over 5,000 years.*

**Table 4-1. Summary of the cases tested in the sensitivity analyses of the 1D fracture model presented in Table 2-6. Groundwater velocity (v), porosity (ϕ), percentage of iron initially present in the fracture filling minerals of the fracture (%$Fe_2O_3$), surface area of annite considered ($S_A$) and ferric secondary mineral precipitate (Fe-prec.) are indicated. HFO stands for hydrous ferric oxide ($Fe(OH)_3$(am)) and Hem for hematite (α–$Fe_2O_3$). Parameter changes with respect to the reference case are displayed in bold. Eh indicates the redox potential reached at 400 m after the simulation time ($t_{sim}$).**

| Case | | v (m/s) | ϕ (–) | %$Fe_2O_3$ | Annite (mol/L) | Calcite (mol/L) | $S_A$ [1] ($m^2$/L) | Fe-prec. | $t_{sim}$ | Eh (mV) |
|---|---|---|---|---|---|---|---|---|---|---|
| Reference case | | $1{\cdot}10^{-7}$ | 0.2 | 2.5 | 1.125 | 15.52 | 8.64 ($1.5{\cdot}10^{-2}$) | HFO | 5,000 | –365 |
| Sensitivity analysis | | | | | | | | | | |
| Velocity | V5 | **$1{\cdot}10^{-5}$** | 0.2 | 2.5 | 1.125 | 15.52 | 8.64 ($1.5{\cdot}10^{-2}$) | HFO | 100 | –363 |
| | V6 | **$1{\cdot}10^{-6}$** | 0.2 | 2.5 | 1.125 | 15.52 | 8.64 ($1.5{\cdot}10^{-2}$) | HFO | 5,000 | –369 |
| | V8 | **$1{\cdot}10^{-8}$** | 0.2 | 2.5 | 1.125 | 15.52 | 8.64 ($1.5{\cdot}10^{-2}$) | HFO | 5,000 | –361 |
| | V9 | **$1{\cdot}10^{-9}$** | 0.2 | 2.5 | 1.125 | 15.52 | 8.64 ($1.5{\cdot}10^{-2}$) | HFO | 15,000 | –354 |
| Porosity2 | | $1{\cdot}10^{-7}$ | **0.1** | 2.5 | **2.25** | **35** | 8.64 ($1.5{\cdot}10^{-2}$) | **Hem** | 120 (3) | –192 |
| %Fe2 | | $1{\cdot}10^{-7}$ | 0.2 | **17.5** | **7.875** | 15.52 | 8.64 ($1.5{\cdot}10^{-2}$) | **Hem** | 5,000 | –377 |
| Min2 | | $1{\cdot}10^{-7}$ | 0.2 | 2.5 | 1.125 | 15.52 | 8.64 ($1.5{\cdot}10^{-2}$) | **Hem** | 5,000 | –241 |
| $S_A$ of annite | SA-1 | $1{\cdot}10^{-7}$ | 0.2 | 2.5 | 1.125 | 15.52 | **1 ($1.7{\cdot}10^{-3}$)** | **Hem** | 120 (3) | –192 |
| | SA-4 | $1{\cdot}10^{-7}$ | 0.2 | 2.5 | 1.125 | 15.52 | **4 ($6.9{\cdot}10^{-3}$)** | **Hem** | 5,000 | –363 |
| | SA-20 | $1{\cdot}10^{-7}$ | 0.2 | 2.5 | 1.125 | 15.52 | **17 ($2.9{\cdot}10^{-2}$)** | **Hem** | 5,000 | –370 |

[1] Values in parenthesis are A, surface area expressed in $m^2$/g.

### *Influence of hydrodynamic parameters: influence of groundwater velocity*

It has been highlighted in the description of the conceptual model that flow velocity influences the advancement of the oxygenated water. If water flux is high, the kinetically controlled dissolution of annite may not be able to supply enough Fe(II) to consume the oxygen and the oxidant front will travel a longer distance. V5, V6, V8 and V9 cases are compared to the reference case and analysed (see Table 4-1 for cases details).

Figure 4-11 shows the penetration of oxygen after 100 and 1,500 years of simulation for four different groundwater velocities between $10^{-5}$ and $10^{-8}$ m/s. Note that oxygen does not reach repository depths in any cases. As expected, the higher the flow velocity, the faster the oxygen intrusion and the deeper the oxidant front.

The comparison between the influxes of oxygen with the rate of oxygen consumption due to the oxidation of Fe(II) released from annite are shown in Table 4-2. First, the oxygen flowrate at the boundary increases with groundwater velocity. However, groundwater velocity is implemented in the code as the rate of water replacement of each cell. Therefore, to vary flow velocity, the user changes the time of water replacement, i.e. the time step. The higher the water flux, the shorter the time step, space discretisation remaining the same for each case. The oxygen concentration entering at the top boundary stays $2.34{\cdot}10^{-4}$ mol/L in each case. As soon as oxygen enters in the system, pH raises up to 9.8. At this pH, the release of iron, independent of flow velocity (equation 2-4), is $4.16{\cdot}10^{-11}$ $mol{\cdot}L^{-1}{\cdot}s^{-1}$. Furthermore, oxygen depletion depends on the oxidation and precipitation of iron, which are in equilibrium. Hence, the stoichiometric relation gives 4 mol of oxygen consumed for each mol of iron released independently of water flux. The concentration of consumed oxygen during a time step, which depends on flow velocity, fluctuates. As a consequence, the buffering of the oxygen front will be effective only in those cases where the consumption of oxygen due to Fe(II) oxidation ($R_{O2}$) is close to, or higher than, the oxygen influx due to melting water infiltration. In these cases (groundwater velocity lower than $10^{-7}$ m/s), the oxygen does not enter into the domain.

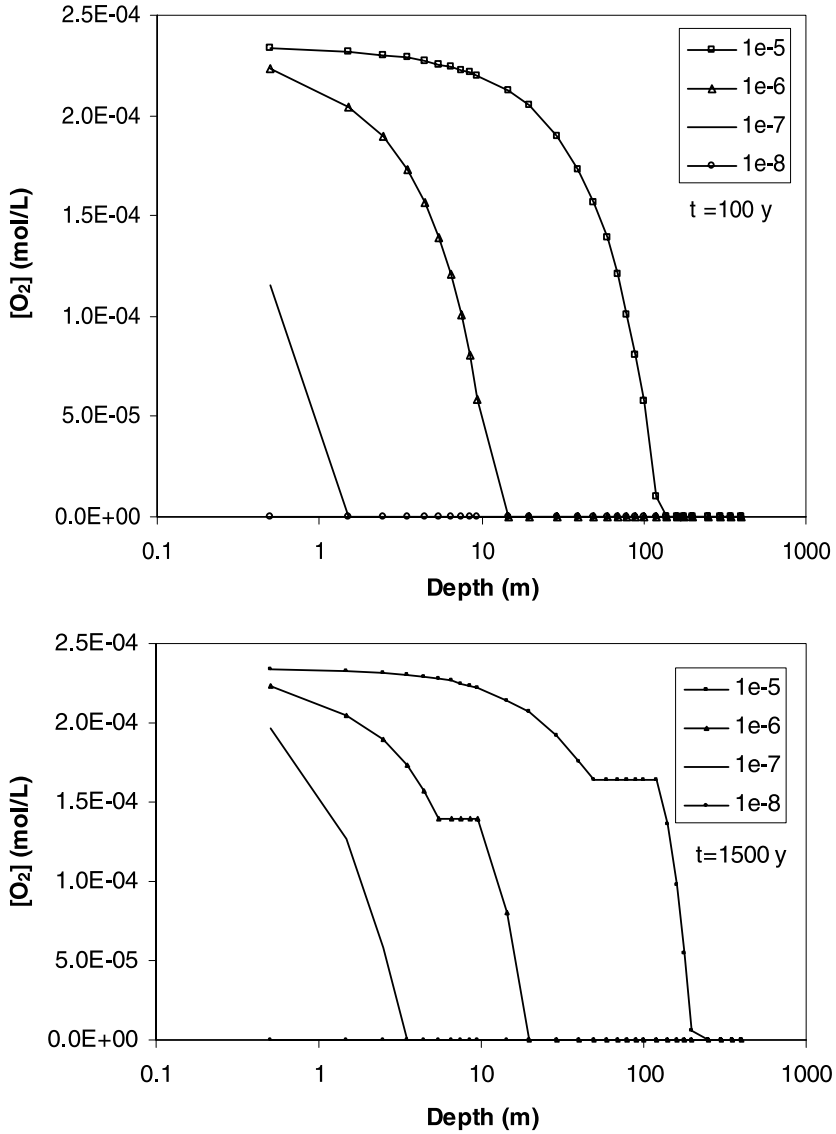


***Figure 4-11.*** *Penetration depth of oxygen after 100 years and 1,500 years of simulation at different groundwater velocities.*

**Table 4-2. Comparison between oxygen flux due to melting water infiltration and oxygen consumption due to Fe(II) dissolution from annite and redox potential after the period of simulation as in Table 4-1. $t_{ADV}$ stands for the advective time (distance/groundwater velocity).**

| v (m/s) | $10^{-5}$ | $10^{-6}$ | $10^{-7}$ | $10^{-8}$ | $10^{-9}$ |
|---|---|---|---|---|---|
| $R_{O2\text{-}infl}$ [1] (mol $O_2$/(s L)) | $2.34\cdot10^{-9}$ | $2.34\cdot10^{-10}$ | $2.34\cdot10^{-11}$ | $2.34\cdot10^{-12}$ | $2.34\cdot10^{-13}$ |
| Δt(s) | $10^5$ | $10^6$ | $10^7$ | $10^8$ | $10^9$ |
| **Oxygen concentration influx at the boundary per time step (mol $O_2$/L)** | **$2.34\cdot10^{-4}$** | **$2.34\cdot10^{-4}$** | **$2.34\cdot10^{-4}$** | **$2.34\cdot10^{-4}$** | **$2.34\cdot10^{-4}$** |
| $R_{Fe}$ release [2] (mol Fe/(s L)) | $4.16\cdot10^{-11}$ | $4.16\cdot10^{-11}$ | $4.16\cdot10^{-11}$ | $4.16\cdot10^{-11}$ | $4.16\cdot10^{-11}$ |
| $R_{O2}$ [3] (mol $O_2$/(s L)) | $1.04\cdot10^{-11}$ | $1.04\cdot10^{-11}$ | $1.04\cdot10^{-11}$ | $1.04\cdot10^{-11}$ | $1.04\cdot10^{-11}$ |
| **$R_{O2}\cdot\Delta t$: oxygen consumption per time step at pH = 9.8 (mol/L)** | **$1.04\cdot10^{-6}$** | **$1.04\cdot10^{-5}$** | **$1.04\cdot10^{-4}$** | **$1.04\cdot10^{-3}$** | **$1.04\cdot10^{-2}$** |
| Eh (mV) | −363 | −369 | −365 | −361 | −354 |
| $t_{ADV}$ (years) | 1 | 13 | 127 | 1,268 | 12,684 |
| depth of $O_2$ penetration (m) after the simulation period ($t_{sim}$) | 250 | 50 | 4.5 | 0 | 0 |
| $t_{sim}$ (years) | 2,000 | 5,000 | 5,000 | 5,000 | 15,000 |

[1] Rate of $O_2$ inflow [mol $O_2$/(s L)]
Flux of $O_2$ [mol/(s L)] = v [m/s]·$[O_2]_{boundary}$[mol/L]
With $[O_2]_{boundary}$ (oxygen concentration at the boundary) = $2.34\cdot10^{-4}$ mol/L

[2] $R_{Fe}$: Fe(II) release [mol Fe/(s L)]
$R_{Fe}$ [mol/(s L)] = $R_{Fe}$ [mol/($m^2$ y) defined in eq 2.3 in Table 2-3]·$S_A$[$m^2$/L]/conversion of year into seconds [y/s]
The highest pH obtained are 9.8, therefore $R_{Fe}$ = 0.000152 mol/($m^2$ y) ratio of iron dissolution (mol/(s L)) = 0.000152 mol/($m^2$ y)·8.64 $m^2$/L/(365.25·86,400 s/y) = $4.16\cdot10^{-11}$ mol/(s L)

[3] $R_{O2}$ oxygen consumption rate[mol $O_2$/(s L)]
According to the oxidation law for iron, 3 mole of $Fe^{3+}$ need 0.75 mole of $O_2$. Hence, each mol of $Fe^{2+}$ consumes 4 mole of $O_2$
Hence, $R_{O2} = 4.16\cdot10^{-11}/4 = 1.04\cdot10^{-11}$ mol/(s L)

In cases of very fast annite dissolution, the depth of oxygen penetration can be calculated analytically and compared to the results presented in Table 4-2. The reductive capacity of the system is the capacity of the system to consume oxydants given by the presence of iron(II) in the reducing minerals. Assuming that reducing minerals are exclusively annite, the reducing capacity of the system (RDC) is formulated as follow:

$$RDC = \frac{mol_{Fe}}{L} \cdot \nu_{annite} \qquad \text{equation 4-1}$$

with $\nu_{annite}$ the stoichiometric factor of oxygen in the process of annite oxidation.

RDC is expressed as a function of the iron content in Forsmark fracture (moles of iron per one litre of water; see equation 2-1) by $\nu_{annite}$, whose value is ¼. This expression is true in cases annite dissolution is very fast. Then, RDC is 0.084 $mol_{O2}$/L considering the porosity (0.2) and the amount of $Fe_2O_3$ (2.5%) to calculate the iron content in cases V5 to V9 (see Table 4-1).

Let assume a cell of our domain (1L contained in a 1 metre long cell). The oxygen front will flow through the cell only once annite is totally consumed. The time needed to deplete oxygen is proportional to RDC ($mol_{O2}$/L) and the flux of oxygen inflow ($R_{O2\text{-}infl}$). Therefore, the time needed to consume the reducing capacity contained in a cell of 1 metre long is:

$$t_d = \frac{RDC}{R_{O2-infl}} \qquad \text{equation 4-2}$$

with $R_{O2-infl} = v \cdot [O_2]$ equation 4-3

The time for the oxygen front to go through a cell of 1 metre, $t_{OF}$, is the sum of the time for oxygen depletion ($t_d$) and the time necessary for oxygen to advance 1 metre ($t_a$). Then, the velocity of advancement of the oxygen front is the inverse of $t_{OF}$ previously defined. Therefore, we can estimate the distance reached by the oxygen front at the simulation time for each sensitivity case onto flow velocity, see Table 4-3.

As can be observed, there is a very good agreement between the simulated and calculated depth of oxygen penetration. The hypothesis of very fast annite dissolution causes some difference for the fastest flow velocity. Assuming an instantaneous dissolution of the mineral implies that the advancement of the oxygen front is possible only once the total amount of RDC is oxidized in a cell. However, iron(II) release follows a kinetic law. Therefore, if flow velocity is very fast in comparison with the rate of release, oxygen advances earlier to the following cell, and the front progresses deeper.

Results indicated in Table 4-2, show that the consumption of oxygen will not be completely buffered by the release of iron for velocities faster than $10^{-7}$ m/s. It is important to note that this effect is constrained in the upper part of the domain, since as indicated in the same table, the redox state remains by far reducing after the periods of simulation. This effect can be seen in Figure 4-12, where the evolution of annite content left in the domain is shown for the case where the flux is $10^{-8}$ and $10^{-6}$ m/s. Under this former flow conditions, the complete depletion of annite occurs after 1,500 years locally between 5 and 10 metres (far from the repository depth), due to the intrusion of the oxygen. However, oxygen is completely consumed in the reference case within the first 5 metres of the domain after 5,000 years, as well as in those cases with lower flow-rates. Furthermore, after the periods of simulation, the annite remaining in the domain is capable of continuing to buffer the ingress of oxygen since it is not depleted at the repository depths. This is consistent with the values reported in Table 4-2.

Figure 4-13 indicates the different redox potential values reached after 1,000 years of simulation and confirms that velocities lower than the reference imply sufficient time for annite to buffer the oxidant intrusion, that is, to maintain the redox potential in reductive conditions. For groundwater velocities of $10^{-6}$ m/s, after 1,000 years the oxidant front has travelled a distance of 10 m, in comparison with the progress of 2 m in the reference case (see also Figure 4-6). In any case, the oxygen will not reach repository depths during the deglaciation period, which is estimated in 5,000 years. This will not happen in any of the cases tested in the sensitivity analyses conducted in this work.

**Table 4-3. Intermediate calculation steps to estimate analytically the depth of oxygen penetration for different groundwater velocities. Comparison with the numerical results.**

| v (m/s) | $10^{-5}$ | $10^{-6}$ | $10^{-7}$ | $10^{-8}$ | $10^{-9}$ |
|---|---|---|---|---|---|
| $R_{O2\text{-}infl}$ ($mol_{O2}$/(s L)) | $2.34 \cdot 10^{-9}$ | $2.34 \cdot 10^{-10}$ | $2.34 \cdot 10^{-11}$ | $2.34 \cdot 10^{-12}$ | $2.34 \cdot 10^{-13}$ |
| $t_d$ (y) | 11.4 | 114.29 | 1,142.9 | 11,429 | 114,293 |
| $t_a$ (y) | $3.17 \cdot 10^{-3}$ | $3.17 \cdot 10^{-2}$ | $3.17 \cdot 10^{-1}$ | 3.17 | 31.7 |
| $t_{OF}$ (y) | 11.4 | 114.32 | 1,143.21 | 11,432.17 | 114,324.7 |
| $v_{OF}$ (m/y) | $8.77 \cdot 10^{-2}$ | $8.75 \cdot 10^{-3}$ | $8.75 \cdot 10^{-4}$ | $8.75 \cdot 10^{-5}$ | $8.75 \cdot 10^{-6}$ |
| $t_{sim}$ (y) time of simulation | 2,000 | 5,000 | 5,000 | 5,000 | 15,000 |
| Depth of $O_2$ penetration (m) calculated analytically | 175 | 44 | 4.4 | 0.4 | 0.1 |
| Depth of $O_2$ penetration (m) obtained numerically | 250 | 50 | 4.5 | 0 | 0 |

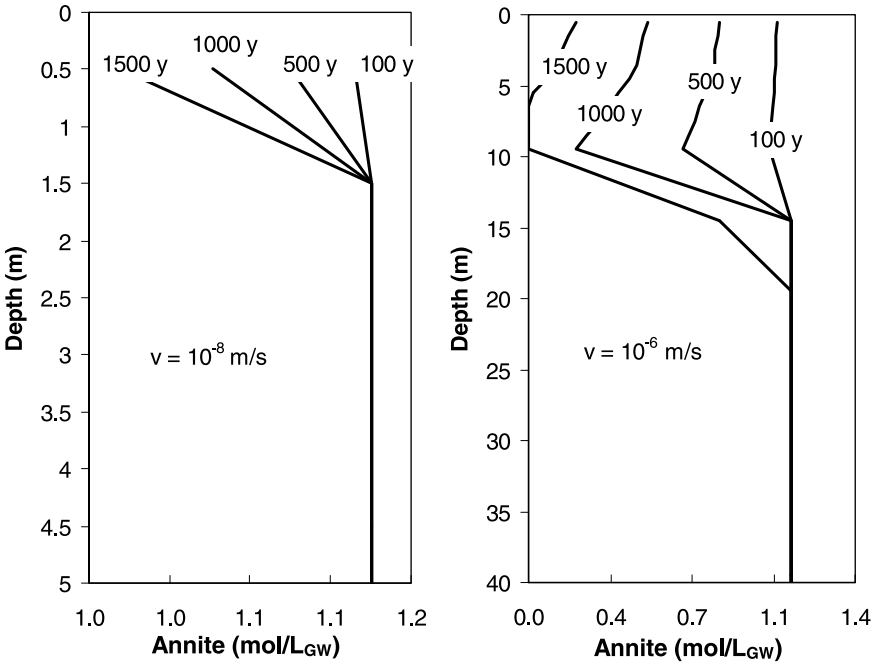


***Figure 4-12.*** *Evolution of annite content in the system for higher and lower velocities than the reference case. Note the different scales in the vertical axis (depth).*

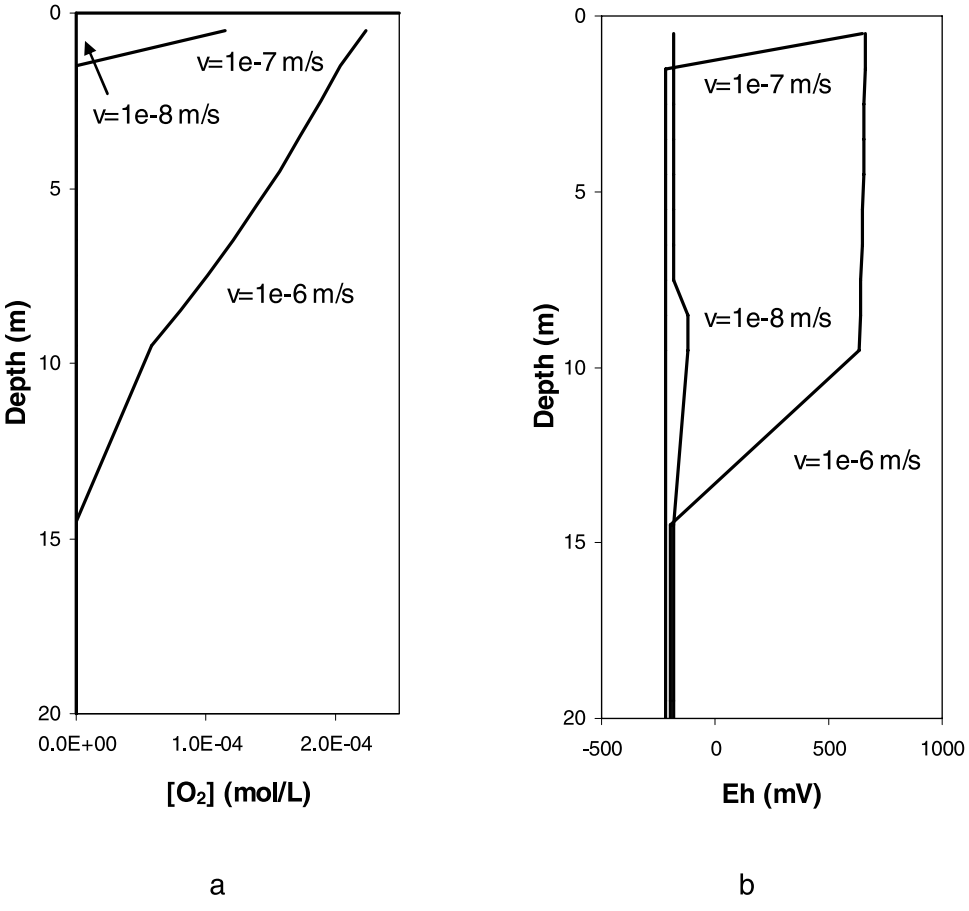


***Figure 4-13.*** *Values of redox potential (a) in the domain and oxygen concentration (b) after 1,000 years for two velocities different from the reference case.*

Figure 4-14 shows that dissolved oxygen advances down to 20 m in 25 days at a groundwater velocitiy of $10^{-5}$ m/s, but no annite is dissolved. During such a short period, oxygen flowrate is too fast with respect to mineral dissolution.

From then, the oxygen front is still going deeper, but some annite starts dissolving. The profiles of oxygen present a peak, which corresponds to a high value of dissolved oxygen compared to the previous node of the domain. This relatively high oxygen content is related to the followed situation: the oxygen has just reached this depth, but no annite has been dissolved yet to buffer it. A steady state of the oxygen front is reached after 5 months considering such a high flow velocity due to the slow dissolution of annite. This front is maintained over 1,000 years. After then, the annite content is totally consumed at 120 metres. Therefore, the oxygen front advances deeper again (Figure 4-15).

It is shown that for 2,000 years, the maximum simulation time, oxic conditions ($[O_2] > 10^{-6}$ mol/$L_{gw}$) reach a depth of 250 m. Then, it is reasonable to assume that under these specific circumstances, oxic conditions could reach repository depths after 5,000 years.

The pH increases with depth up to 120 metres (Figure 4-15). Similarly to the cases for groundwater velocity of $10^{-6}$ m/s, since the rate of dissolution being proportional to pH, annite is dissolved mainly at 120 metres (Figure 4-13, Figure 4-15). This explains why the content of annite is higher in the first metres of the domain than at 120 metres, where less oxygen is present.

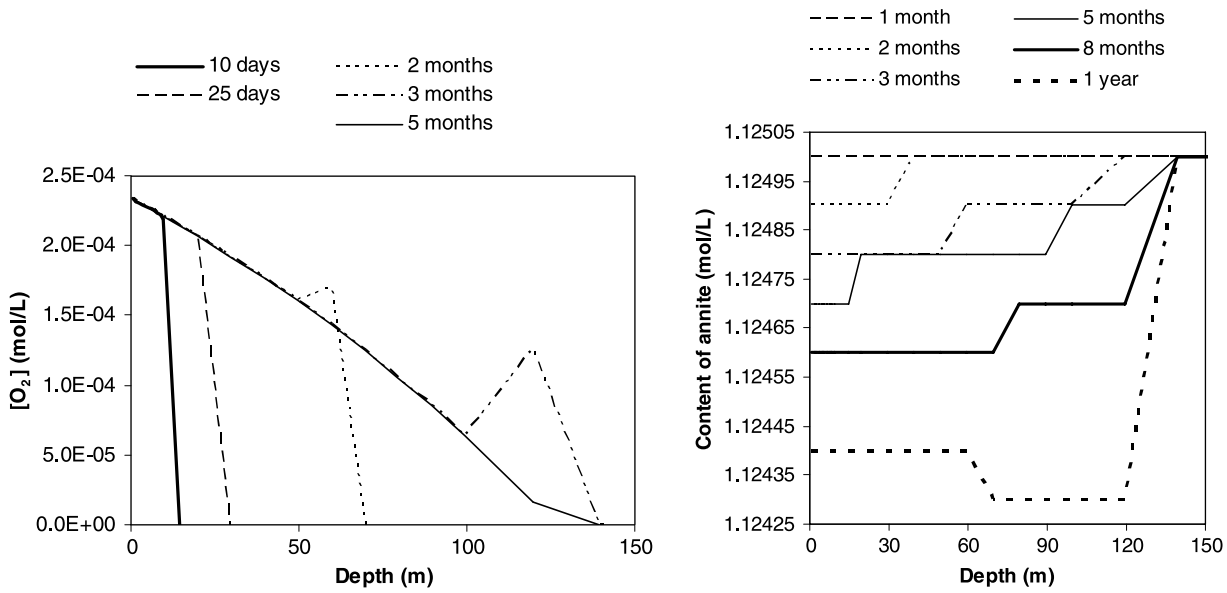


***Figure 4-14.*** *Evolution of the oxygen front at early times ($v = 10^{-5}$ m/s). Note the change in the scale in years axis.*

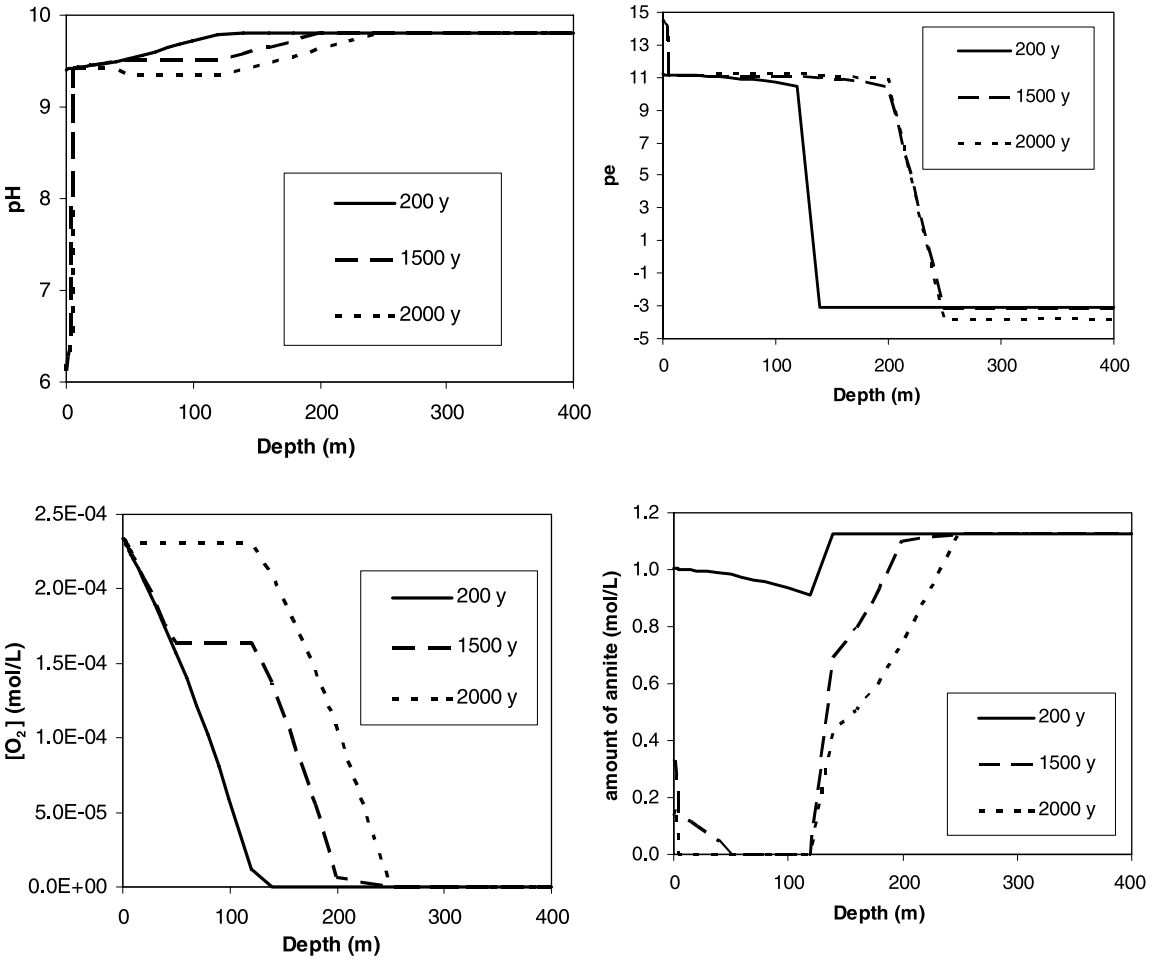


***Figure 4-15.*** *Evolution of the master variables, oxygen front and annite for $v = 10^{-5}$ m/s.*

### *Sensitivity analysis on geochemical parameters: influence of the Fe(III) precipitate*

The ferric mineral that could precipitate in this case is Hematite ($Fe_2O_3$) instead of the more amorphous ferric hydroxide ($Fe(OH)_3$) considered in the reference case (see in Table 4-1 case Min2 for details).

The main difference in this case is that the final redox potential in the system is lower in the case of considering hematite, given that this solid is thermodynamically more stable. Whereas in the reference case, the redox potential is kept to values around –180 mV, in the case of considering hematite it reaches values around –360 mV. This is explained by the different final equilibrium established in the system (see Figure 4-16).

The precipitation/dissolution of hematite and $Fe(OH)_3$(am) are in equilibrium in both cases. Therefore, the amount of hematite precipitated is half that of $Fe(OH)_3$(am) formed in the reference case to consume the same amount of Fe(III) generated by the oxidation of Fe(II) released by annite dissolution.

### *Sensitivity analysis on geochemical parameters: influence of the Fe(II)-bearing mineral content*

When the initial amount of annite in the system is increased by a factor of 7 (see in Table 4-1 case %Fe2 for details), there is enough mineral to buffer the oxygen intrusion along the whole domain during the 5,000 years period and it does not become depleted with time. The system remains invariant.

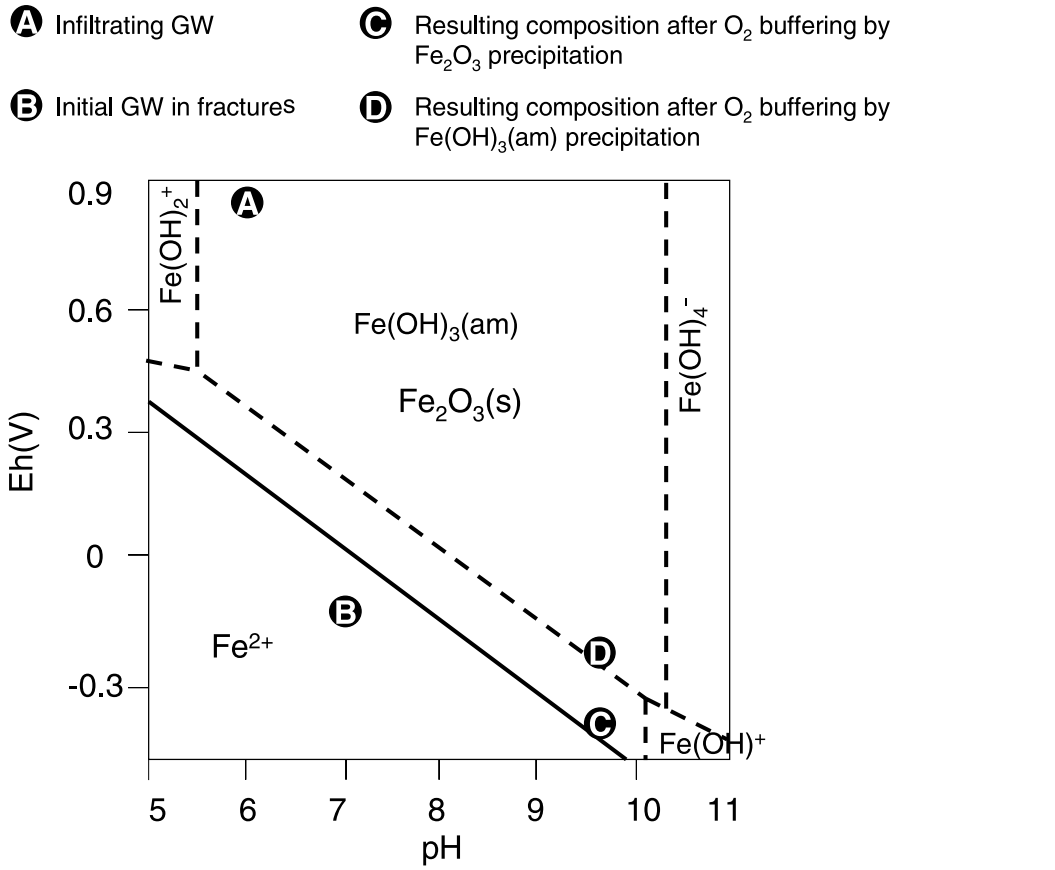


***Figure 4-16.*** *Eh-pH diagram of the system depending on whether amorphous $Fe(OH)_3$ or cristalline hematite ($Fe_2O_3$(s)) are considered to form as secondary solid phases. Dashed lines stand for the predominance diagram in the case of inhibiting the precipitation of hematite.*

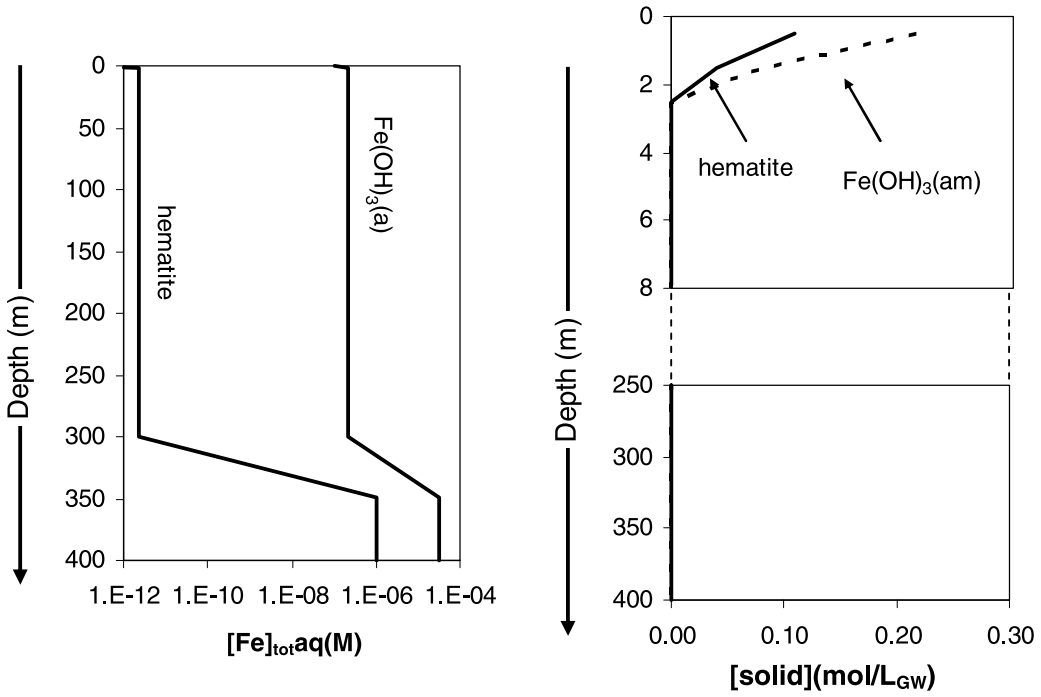


***Figure 4-17.*** *Comparison of the total aqueous iron concentration and the content of Fe(III) precipitate at 5,000 years.*

***Sensitivity analysis on geochemical parameters: influence of the surface area***

As commented in the description of the conceptual model, the surface area ($S_A$) is a very uncertain parameter. The value of $S_A$ implemented into the model may be representative of the accessibility of the mineral. The higher the surface area, the faster the annite dissolution. This is expressed by equation 3-1. Therefore, we realised a sensitive analysis on this parameter (see cases SA-1, SA-4 and SA-20 in Table 4-1 for details).

Figure 4-18 helps in comparing the dissolved oxygen and annite content profiles between cases SA-4 ($S_A = 4$ m$^2$/L), SA-20 ($S_A = 17$ m$^2$/L) and the reference case ($S_A = 8.64$ m$^2$/L). The lower the surface area, the slower the annite dissolution and the deeper the oxidant front. For the lowest surface area case (SA-1, with $S_A = 1$ m$^2$/L), the oxidant front reaches 15 m after 120 years to compare with 2.5 m in the reference case.

It is worth noting that we assign a surface area 100 times lower than the one provided by the literature in the reference case. A surface area only twice as much as the reference case suffices to prevent any intrusion of oxygen at least during 100 years.

## 4.2 Rock system

The concept of the rock system is very similar to the fracture one. The differences are the values of hydrodynamic and geochemical parameters attributed to the system, such as groundwater velocity ($1 \cdot 10^{-9}$ m/s), porosity (0.02%) and annite and calcite contents (2%wt in Fe(II) and 0.4%wt, respectively). It is worth noting that the initial concentration of annite is higher than in the fracture system due to the lower porosity of the rock. As expected, the oxygen does not reach depths further than 2 metres due to the low flow velocities and to the higher content of Fe-bearing minerals that may buffer the redox front (Figure 4-19).

Flow velocity is slower than in the rock system, therefore oxygen is introduced in the domain at a lower velocity and no major jeopardizing of the reducing conditions is expected.

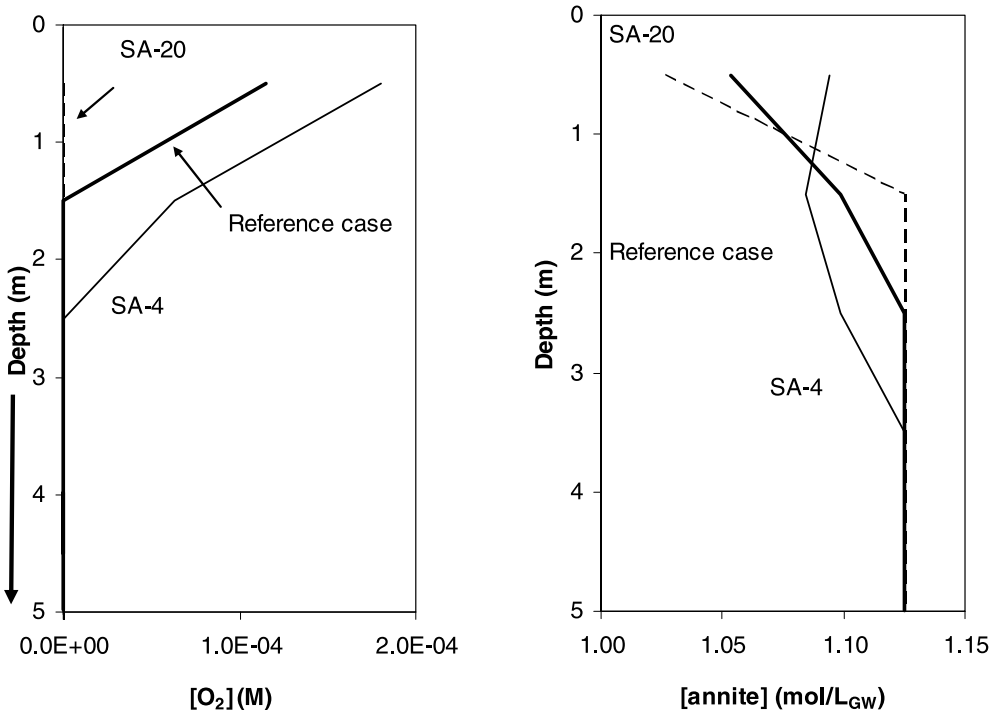


***Figure 4-18.*** *Dissolved oxygen concentration and annite content profiles at 100 years for SA-4 ($S_A = 4$ m$^2$/L), SA-20 ($S_A = 17$ m$^2$/L), and the reference case ($S_A = 8.64$ m$^2$/L). For all cases $v = 10^{-7}$ m/s.*

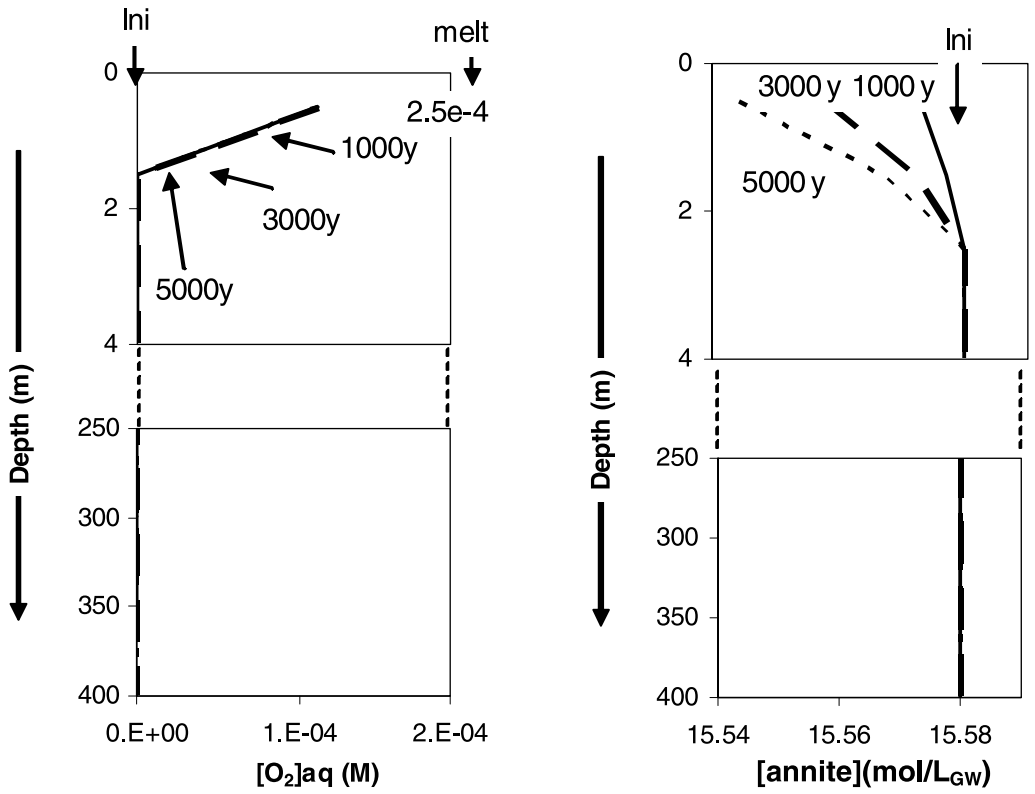


***Figure 4-19.*** *Evolution of dissolved oxygen concentration and the content of annite along the flowpath in the rock system over 5,000 years. "Ini" is the initial water concentration value.*

## 4.3 Conclusions on the 1D models

The main changes induced in the groundwater present in the fracture due to the infiltration of ice-melting water are reflected in Table 4-4.

**Table 4-4. Comparison of the composition of the groundwater in fractures after 5,000 years of the deglaciation period at repository depth with that initially present in the fractures from Forsmark. Concentrations in M.**

| Components | Initial water in fractures | Water in fractures after 5,000 years of deglaciation |
|---|---|---|
| pH (–) | 6.9 | 9.8 |
| Eh (mV) | –189 | –240 |
| $[Na^+]_{tot}$ | $8.88 \cdot 10^{-2}$ | $6.90 \cdot 10^{-4}$ |
| $[K^+]_{tot}$ | $8.75 \cdot 10^{-4}$ | $3.18 \cdot 10^{-4}$ |
| $[Ca^{2+}]_{tot}$ | $2.33 \cdot 10^{-2}$ | $2.17 \cdot 10^{-4}$ |
| $[Mg^{2+}]_{tot}$ | $9.30 \cdot 10^{-3}$ | $6.20 \cdot 10^{-7}$ |
| $[HCO_3^-]_{tot}$ | $2.03 \cdot 10^{-3}$ | $9.28 \cdot 10^{-5}$ |
| $[Cl^-]_{tot}$ | $1.53 \cdot 10^{-1}$ | $4.04 \cdot 10^{-4}$ |
| $[S]_{tot}$ | $6.80 \cdot 10^{-3}$ | 0 * |
| $[Br^-]_{tot}$ | $2.98 \cdot 10^{-4}$ | $3.80 \cdot 10^{-7}$ |
| $[Si]_{tot}$ | $2.67 \cdot 10^{-4}$ | $5.60 \cdot 10^{-4}$ |
| $[Fe]_{tot}$ | $1.00 \cdot 10^{-6}$ | $2.91 \cdot 10^{-7}$ |
| $[Al]_{tot}$ | $5.23 \cdot 10^{-9}$ | $2.71 \cdot 10^{-6}$ |

* Not considered in melting water and complete renovation achieved.

The main changes affect the values of pH, which is higher than initially due to the dissolution of calcite caused by the infiltration of groundwater subsaturated with this solid. This process also has an effect on the concentration of calcium and carbonate. The value of redox potential decreases due to the different processes of oxygen consumption and the release of iron(II) from the dissolution of annite. Other changes worth to comment on are the concentrations of iron and aluminum. Total iron concentration decreases after precipitation and, as we have previously presented its concentration is determined by the equilibration with iron(III) hydroxide under the conditions of the water. Aluminum concentration increase is due to the equilibration with kaolinite under the specified conditions. The concentration of silica is very similar to the initial one, as it is given by equilibration of the system with chalcedony.

In any case, it is foreseen that neither oxygen nor the oxidizing front reaches repository depths in the 5,000 years of the deglaciation period simulated (see Figure 4-6). A rough calculation of the velocity of the oxidation front indicates that, for groundwater rates of $10^{-7}$ m/s, oxidizing conditions have advanced a depth of 5 metres in 5,000 years, that is, the velocity of the redox front is on the order of $10^{-3}$ m/year. For faster velocities, given the lower effect of the annite dissolution on the oxygen consumption, faster advances of the redox front are obtained. Nevertheless, they are never as fast as to reach repository values in 5,000 years. Qualitatively, one could infer that under such rate of progression, the front would reach the repository in 400,000 years; recall that continuous infiltration of oxygenated melt water should happen to maintain this rate, which is rather unlikely and has not been reported yet anywhere.

This oxidizing front advance will depend on the water flow rate and also on the amount of minerals providing reducing capacity to the media. In the case we have been dealing with, the only mineral considered has been annite, as an exemplification of Fe(II)-bearing silicates. Nevertheless, in the case of considering not only the fracture system, but also the matrix one, pyrite may be considered as an important contributor to the reducing capacity.

The oxidation of pyrite can have, a priori, two implications: 1) additional oxygen consumption and 2) acidification of the media. This effect may be reflected in a lower increase of the pH of the system accompanying calcite dissolution.

# 5 Discussion

After presenting and discussing the results obtained in the calculations pertinent for this report, it is convenient to put these results in the context of former and similar calculations /Guimerà et al. 1999/, suggestions to those calculations /Gascoyne 1999/ and implications for the performance assessment of the repository.

The geochemical database used in the present calculations is far more complete (PHREEQC) that the set of equations used previously (Tables 4-1 and 4-2 of /Guimerà et al. 1999/). Therefore, the results obtained from the work reported in this document are slightly different from the ones reported in /Guimerà et al.1999/, although consistent in terms of advective transport. One of the recommendations from /Gascoyne 1999/ was to use mineral contents and hydraulic parameter distributions in agreement with the results of the new site investigation program. A more adequate ice melt water composition in terms of major geochemistry and oxygen content was proposed in his report. While the former and the latter have been easily taken into account, the variability of hydraulic parameters with depth was no accounted for in 1D models.

As indicated in Table 2-7, the reducing capacity considered in this work is lower than the one taken into account in /Guimerà et al. 1999/. Besides, the concentration of oxygen in the melt water used in this study is lower than the one used previously. Oxygen does not reach repository levels – neither did it in the former calculations – but in this case, the results of the model do not show high redox potentials at repository depth, in opposition to the results obtained in 1999. This is illustrated in Figure 5-1 and Figure 5-2, where the redox potential (in terms of pe = Eh/59.16 mV) obtained with the former model is compared with the present results.

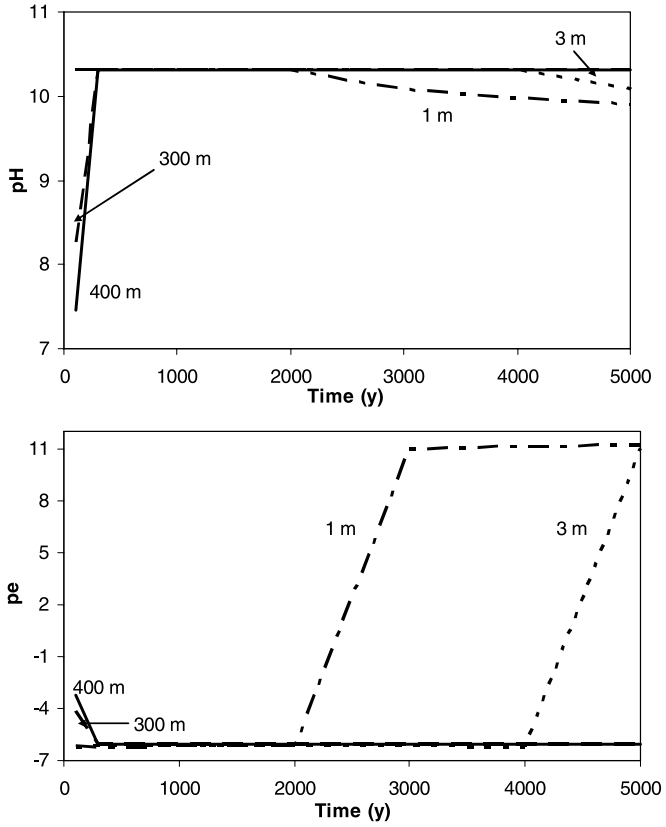


***Figure 5-1.*** *Master variables of the reference case of this report after the period of simulation for four given altitudes. 400 m represents the repository level. Note that the redox state (in terms of pe = Eh/(59.16 mV)) does not vary, reflecting that neither oxygen nor any other oxidant reaches the repository depth.*

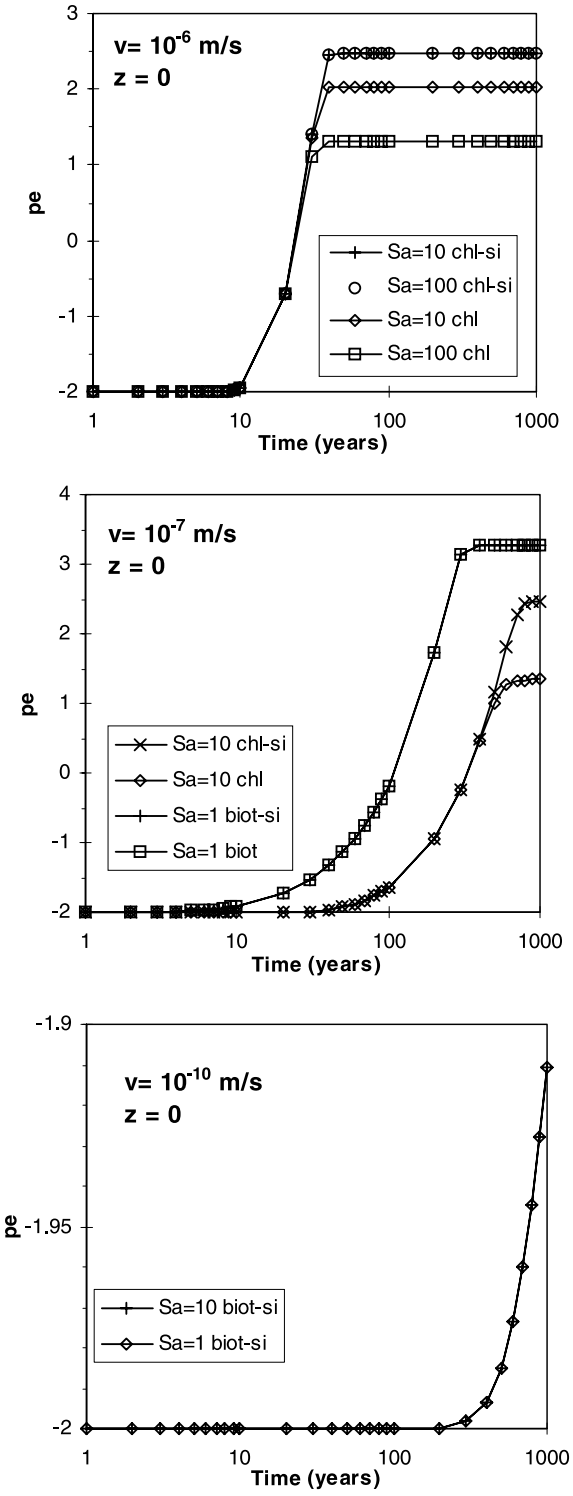


***Figure 5-2.*** *Redox state for the former project /after Guimerà et al. 1999/ for different groundwater velocities and mineral contents. Calculations for the repository level. Note that the coordinate system differs from the one used along this report. In this plot z=0 means repository level.*

This report does not present many results nor discussion on the uncertainty of $S_A$ which was deemed to be crucial in the report of /Guimerà et al. 1999/. In fact, not much has been gained since then and the way in which the analyses where performed in that project reflected the convenience of a proper sensitivity analysis to deal with it. Due to the more conservative value used for the surface area, the sensitivity analyses in this sense is not as extensive in the present report. As stated in Chapter 2, we are using a value two orders of magnitude lower than the result obtained experimentally by /Mälstrom et al. 1994/ or by /Samson et al. 2005/. Hence, even in the most pessimistic scenario – low mineral content, fast groundwater velocity – the "real" surface area should still be 100 times larger than that used here, which should enhance the buffering capacity of the system to a certain extent. As a result, even in the most pessimistic scenario, no oxygen will present at repository depths and the system will remain under reducing conditions.

In the model calculations the surface area of reacting Fe(II)-mica has been set to ≈ 9 $m^2/L$ (see Section 2.5), simulating a fracture containing gouge material. The amount of Fe(II) in this mineral, reflecting the total capacity of the fracture to consume the incoming $O_2$, is according to Table 2-2 equal to (3×1.125) $mol/L_{water}$.

In the case of a fracture not containing any fracture filling mineral, it is of interest to estimate the depth of rock necessary to provide a similar amount of reducing capacity. The reference case (fracture porosity of 0.2 and annite content 1.125 $mol/L_{water}$) will be illustrated here.

Let's consider a unit cell of fracture implemented in the 1D model, of 1 metre long and containing 1 $dm^3$ of water. We can consider that the aperture of the fracture is of $0.5 \cdot 10^{-3}$ m and therefore, with a porosity of 0.2, its width is of 10 metres (see Figure 5-3).

The quantity of annite in the cell representing the fracture is of 1.125 moles.

In the rock matrix, we have 15.58 moles of annite per $dm^3$ of water, and the porosity of the matrix is 0.02. This means that to have a reducing capacity in the host rock equivalent to that in the hypothetical fracture cell considered above, we need a volume of host rock matrix of:

$$1.125 \text{ mol annite} \cdot \frac{\text{dm}^3 \text{ water in host rock}}{15.58 \text{ moles annite}} \cdot \frac{1 \text{ dm}^3 \text{ host rock}}{0.02 \text{ l water in host rock}} = 3.61 \text{ dm}^3 \text{ host rock}$$

And considering that the surface of the fracture is $10 \cdot 1 = 10$ $m^2$, we need a depth of host rock to provide an equivalent reducing capacity of:

$$\frac{3.61 \text{ dm}^3 \text{ host rock}}{10 \text{ m}^2} \cdot \frac{1 \text{ m}^2}{100 \text{ dm}^2} = 3.61 \cdot 10^{-3} \text{ m of host rock depth}$$

That is, an equivalent depth of 0.18 mm per fracture surface (see Figure 5-4).

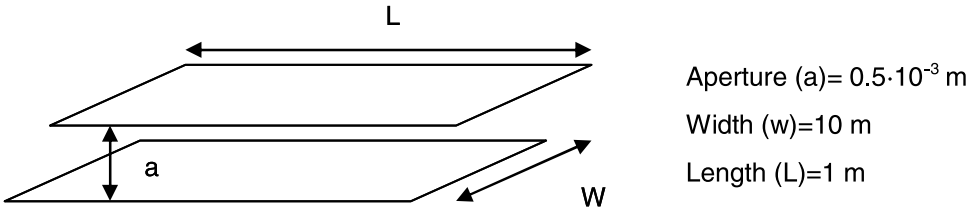


***Figure 5-3.*** *Schematic view of an open fracture whose length, width and aperture are respectively 1 m, 10 m and 0.5 mm.*

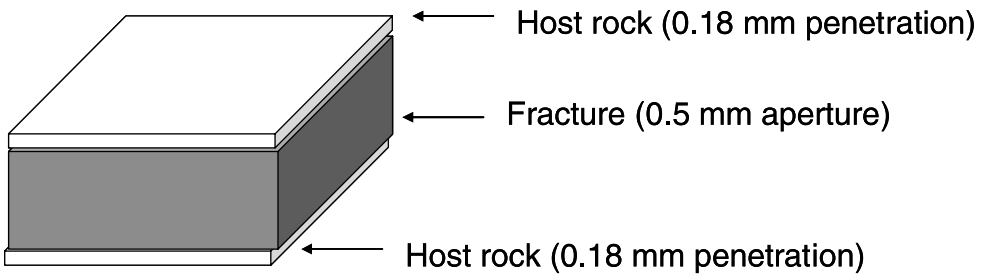


***Figure 5-4.*** *Sketch showing the depth of matrix needed to provide a reducing capacity equivalent to that of the fracture modelled in the base case.*

A major contribution and clarification of this report is that while in former calculations, oxygen was scavenged but at repository depth relatively high redox potentials, up to +180 mV, could be reached, the present calculations show that oxygen is also efficiently scavenged and the redox conditions remain almost invariant for the period of simulation. That is, the redox potential at repository depth remains equally reducing, in the range from –180 to –360 mV.

The chemical composition of groundwater varies from the initial infiltration water as shown in Table 4-4 and presented in Figure 5-5 for illustrative purposes. The results show an increase of pH in the groundwater surrounding the repository, from 6.9 to 9.8, a decrease in the redox potential, from –189 to –249 mV and a general decrease in the concentrations of all the major elements in solution, what is in agreement with the dilution caused by the much less mineralised water resulting from ice melting.

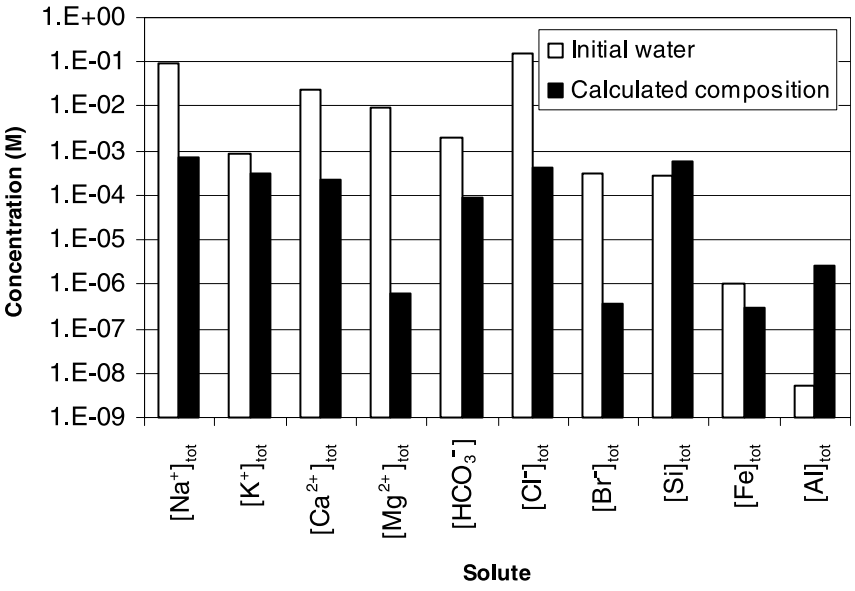


***Figure 5-5.*** *Changes in chemical composition of groundwater. pH increases from 6.9 to 9.8 and the redox potential decreases from –189 to –240 mV.*

# 6 Conclusions

The impact of melt water in groundwater at repository depths has been assessed by means of conceptual and numerical models based on previous calculations made by /Guimerà 1999/ and suggestions by /Gascoyne 1999/. In addition to the evaluation of the redox front migration and progression of the oxygen content, a complete analysis of the groundwater composition changes has also been done.

A number of cases have been tested, most of them based on different combinations of parameters and domains mimicking processes occurring in fractures and in fractured host rocks as well.

Oxygen becomes depleted in the system before reaching the repository depths during the period of simulation of the reference case, 5,000 years. This is valid for all the rest of the cases tested. In addition, the redox potential around the repository is kept at very low values, indicating that the system is able to buffer the oxic intrusion. This is an important result, in opposition to the results obtained by /Guimerà et al. 1999/ that indicated that oxidizing conditions could reach repository depths. These conditions were for groundwater velocities of $10^{-5}$ m/s, for surface areas ($S_A$) lower than 1 $m^2$/L and for systems not buffered by calcite. Under these situations the redox potential increased from Eh = –120 mV up to 240 or 420 mV, depending on the combination of parameters (see Table 4-6 of that report). The explanation for this is the lower mineral abundance used in the present calculations, in agreement with the results obtained by the site characterisation of Forsmark.

# References


**Adler P M, Thovert J F, 1999.** Fracture and fracture networks. Kluwert, Dordrecht, The Netherlands, 429 pp.

**Ahonen L, T Vieno, 1994.** Effects of glacial meltwater on corrosion of copper canisters. Report YJT-94-13, nuclear waste commission of Finish Power Companies. 20 pp.

**Aksoyoglu S, Bajo C, Mantovani M, 1990.** Grimsel Test Site – Batch Sorption Experiments with Iodine, Bromine, Strontium, Sodium and Caesium on Grimsel Mylonite. Nagra Technical Report NTB 91-06, Nagra, Wettingen, Switzerland (February 1991); PSI Report 83, Paul Scherrer Institute, Würenlingen and Villigen, Switzerland. (December 1990).

**Bajo C, Aksoyoglu S, Mantovani M, 1989.** Groundwater Stability and Rock-water Interaction Experiments. In: BRADBURY, M.H. (ed.) (1989): Grimsel Test Site – Structural Geology and Water Flow Paths in the Migration Shear Zone. Nagra Tech. Report NTB 88-23, Nagra, Wettingen, Switzerland; PSI Report 28, Paul Scherrer Institute, Würenlingen and Villigen, Switzerland.

**Bear J, Tsang C H, de Marsily C (eds.), 1993.** Flow and contaminant transport in fractured rocks. Acad. Press., San Diego, CA, USA, 560 pp.

**Berglund S, Selroos J O, 2004.** Transport properties site descriptive model. Guidelines for evaluation and modelling. SKB R-03-09, Svensk Kärnbränslehantering AB.

**Blomqvist R, S K Frape, Nissinen P, Ivanovich M, Vuorela P, Blyth A, Ruskeeniemi T, 1992.** Crustal rebound-relate groundwater flow and calcite formation in the crystalline bedrock of the Fennoscandian shield: new observations from Finland. Paleohydrogeological methods and their applications. Proc. of NEA workshop, Paris, 9–10/11/92, 161–167.

**Bodin J, Delay F, de Marsily G , 2003.** Solute tranport in a single fracture with negligible matrix permeability: 1. fundamental mechanisms. Hydrogeology Journal, (11): 418–433.

**Boulton G, de Marsily G, 1997.** Hydrogeological aspects of glaciation. in (eds. L. King-Clayton, N. Chapman, L.O. Eriksson, F. Kautsky) Glaciation and Hydrogeology. Workshop of the impact of climate change and glaciations on rock stresses, groundwater flow and hydrochemistry – past, present and future. Stockholm, April 1996, Statens kärnkraftinspektion SKI Report 97:13.

**Carlsson A, Christiansson R, 1987.** Geology and Tectonics of Forsmark. SKB Progress Report SFR 87-04, Svensk Kärnbränslehantering AB.

**Dershowitz W, Winberg A, Hermansson J, Byegard J, Tullborg E-L, Andersson P, Mazurek M, 2003.** Äspö Hard Rock Laboratory. Äspö Task Force on modelling of groundwater flow and transport of solutes. Task 6C. A semi-synthetic model of block scale conductive structures at the Äspö HRL. SKB International progress report IPR-03-13, Svensk Kärnbränslehantering AB.

**Eikenberg J, Bayens B, Bradbury M H, 1991.** The Grimsel Migration Experiment: A Hydrogeochemical Equilibration Test. Nagra Technical Report NTB 90-39. Nagra, Wettingen, Switzerland.

**Fabishenko B, Whiterspoon P A, Benson S.M (eds.), 2000.** Dynamics of fluids in fractured rock. Am. Geophys. Union, Geophys. Monogr. 122:400.

**Fountain A G, 1994.** Borehole water-level variations and implications for the subglacial hydraulics of South Cascade Glacier, Washington State, U.S.A. J. of Glaciology, 40 (135) 293–304.

**Gascoyne M, 1999.** Long-term maintenance of reducing conditions in a spent nuclear fuel repository. A re-examination of critical factors. SKB R 99-41, 56 pp, Svensk Kärnbränslehantering AB.

**Glynn P D, Voss CI, 1999.** SITE-94: Geochemical characterization of Simpevarp ground waters near the Äspö Hard Rock Laboratory. Report SKI-R-96:29, Swedish Nuclear Power Inspectorate, Stockholm, Sweden.

**Grandia F, Domènech C, Arcos D, Duro L, 2005.** Assessment of the oxygen consumption in the backfill Project OXI-SRCan. Geochemical modelling in a saturated backfill. SKB report. Unpub. Svensk Kärnbränslehantering AB.

**Guimerà J, Duro L, Jordana S, Bruno J, 1999.** Effects of ice melting and redox front migration in fractured rocks of low permeability. SKB TR-99-19, 86 pp, Svensk Kärnbränslehantering AB.

**Hummel W, Berner U, Curti E, Pearson F J, Thoenen T, 2002.** Nagra/PSI. Chemical Thermodynamic database 01/01. Universal Publishers. Florida, USA, 565 p.

**Jaquet O, Siegel P, Klemenz W, Lavanchy J M, 2006.** Simpevarp 1.2 – Regional groundwater flow model for a glaciation scenario. SKB report, aproved for publication, 57 pp, Svensk Kärnbränslehantering AB.

**Johnson J, 2000.** LLNL database for PHREEQC code. Revision: 1.14, 'thermo.com.V8.R6.230'.

**Kotelnikova S, Pedersen K, 1999.** The Microbe-REX project. Microbial O2 consumption in Äspö tunnel. SKB-TR-99-17, Svensk Kärnbränslehantering AB.

**Lasaga A C, 1995.** Fundamental approaches in describing mineral dissolution and precipitation rates. In White, A.F. and Brantley, S.L. (eds.) Chemical weathering rates of silicate minerals, Revs. In Mineralogy, vol. 31, 23–83, Min.Soc. Am. Washington, D.C. ISBN 0-939950-38-3.

**Luukkonen A, Pitkänen P, Partamies S, 2004.** Significance and estimations of lifetime of natural fracture mineral buffers in the Olkiluoto edrock. Posiva WR 2004-08.

**Malmström M, Banwart S, 1997.** Biotite dissolution at 25°C: The pH dependence of dissolution rate and stoichiometry, Geochim. Cosmochim. Acta, 61, 2779–2799

**Malmström M, Banwart S, Duro L, Wersin P, Bruno J, 1995.** Biotite and chlorite weathering at 25°C. SKB TR 95-01, Svensk Kärnbränslehantering AB.

**Neretnieks I, 1986.** Some uses for natural analogues in assessing the function of a HLW repository. Chemical Geology, vol. 55, pp.175–188.

**NRC, 1996.** Rock Fractures and Fluid Flow. Contemporary understandings and applications. National Academy Press, Washigon D.C.552 pp.

**Parkhurst D L, Appelo C A J, 1999.** User's guide to PHREEQC (version 2) – A computer program for speciation, batch-reaction, one-dimensional transport and inverse geochemical calculations. U.S. Geological Survey Water Resources investigations report 99-4259. Denver, Colorado.

**Pedersen K, 2000.** Microbial processes in radioactive waste disposal. SKB TR-00-04, Svensk Kärnbränslehantering AB.

**Petersson J, Berglund J, Danielsson P, Wängnerud A, Tullborg E-L, Mattsson H, Thunehed H, Isaksson H, Lindroos H, 2004.** Forsmark site investigation. Petrography, geochemistry, petrophysics and fracture mineralogy of boreholes KFM01A, KFM02A and KFM03A+B, SKB P-04-103, Svensk Kärnbränslehantering AB.

**Priscu J C, Adams E E, Lyons W B, Voytek M A, Mogk D W, Brown R L, McKay C P, Takacs C D, Welch K A, Wolf C F, Kirshtein J D, Avci R, 1999.** Geomicrobiology of Subglacial Ice Above Lake Vostok, Antarctica. Science 10 December 1999:Vol. 286. no. 5447, pp. 2141–2144. DOI: 10.1126/science.286.5447.2141.

**Pruess K, Fabishenko B, Bodvarsson G.S, 1999.** Alternative concepts and approaches for modelling flow and transport in thick unsaturated zones of fractured rocks. J. Contam. Hydrol. 38 (1–3):281–322.

**Puigdomènech I (ed.), 2001.** Hydrochemical stability of groundwaters surrounding a spent nuclear fuel repository in a 100,000 years perspective. SKB TR-01-28, 83 pp, Svensk Kärnbränslehantering AB.

**Puigdomènech I, Ambrosi J P, Eisenlohr L, Lartigue J E, Banwart S A, Bateman K, Milodowski A E, West J M, Griffault L, Gustafsson E, Hama K, Yoshida H, Kotelkinova S, Pedersen K, Michaud V, Trotignon L, Rivas-Pérez J, Tullborg E L, 2001.** O2 depletion in granitic media. The REX project. SKB TR-01-05, 92 pp, Svensk Kärnbränslehantering AB.

**Puigdomènech I , 2004.** HYDRA-MEDUSA. Chemical Equilibrium Software (1.6 Mb). Updated 18-Feb-2004.

**Sahimi M, 1995a.** Flow and transport in porous media and fractured rock, VCH, Weinheim. 482 p.

**Sahimi M, 1995b.** Effect of long-range correlations on transport phenomena in disordered media, AIChE J. 41(2), 229–240.

**Samper J, Molinero J, Yang Ch, Zhang G, 2003.** Redox zone II Coupled modeling of groundwater flow, solute transport, chemical reactions and microbial processes in the Äspö island. Universidade da Coruña. SKB TR-03-16, Svensk Kärnbränslehantering AB.

**Samson S D, Nagy K L, Cotton W B, III, 2005.** Transient and quasi-steady-state dissolution of biotite at 22–25°C in high pH, sodium, nitrate and aluminate solutions. Geochim. Cosmochim. Acta, 69: 399–413.

**Sidborn M, 2003.** Modelling some biochemically mediated processes in rocks. Licentiate Thesis, Department of Chemical Engineering and Technology, Royal Institute of Technology (KTH).

**SKB, 2004.** Interim main report of the safety assessment SR-Can. SKB TR-04-11, Svensk Kärnbränslehantering AB.

**Svensson U, 1999.** Subglacial groundwater flow at Äspö as governed by basal melting and ice tunnels. SKB R-99-38, Svensk Kärnbränslehantering AB.

**Svensson U, Kuylenstierna H O, Ferry M, 2004.** DarcyTools, Version 2.1 Concepts, methods, equations and demo simulations. SKB R-04-12, Svensk Kärnbränslehantering AB.

**Widestrand H, Byegård J, Ohlsson Y, Tullborg E-L, 2003.** Strategy for the use of laboratory methods in the site investigations programme for the transport properties of the rock. SKB R-03-20, Svensk Kärnbränslehantering AB.

**Williams M M R, 1996.** Radionuclide transport in fractured rock. Prog. Nuclear Energy 30(3):243–253.

**Yang Q, Mayewski P A, Linder E, Whitlow S, Twickler M, 1996.** Chemical species spatial distribution and relationship to elevation and snow accumulation rate over the Greenland Ice Sheet. J. of Geophys. Res. 101 (D13):18629–18637.

# Appendix

## Input file: implementation of the reference case into PHREEQC

```
TITLE
        1D Mice1 FFM con mineral reductor la annite.

RATES
                Annite
                -start
                10  rem PARM(1)=A0. surface area in m2/dm-3
                20  if (m <= 0) then goto 200
                30  si_annite = SI ("annite")
                40  if (si_annite >= 0) then goto 200
                50  r1 = 0.069*(ACT("H+"))^0.51
                60  r2 = 5.28e-11*(ACT("H+"))^(-0.65)
                70  rf=r1+r2
                80  rate = PARM(1)*rf
                90  moles=rate*time/(3600*24*365.25)
                200 SAVE moles
                -end

SOLUTION_SPECIES
H2O + 0.01e- = H2O-0.01
       log_k -8

SOLUTION 1-400  initial groundwater (referenced water from Forsmark)
        units           mol/kgw
        pH              7
        Al              1e-15
        Na              8.88e-2
        K               8.75e-4
        Ca              2.33e-2
        Mg              9.3e-3
        Cl              1.53e-1
        S               6.8e-3
        Br              2.98e-4
        Si              1.85e-4
        Fe              3.31e-5
        pe              -2.42
      Alkalinity  1.77e-3  as HCO3

EQUILIBRIUM_PHASES 1-400
        CALCITE         0       15.5
        Chalcedony      0       1e-2
        hematite        0       0
        kaolinite       0       1e-2
        dolomite        0       0

SOLUTION 0  boundary GW (melt water from Grimsel equilibrated with O2)
    units     mol/kgw
    temp      25
    pH        6
    pe        12.5 O2(g)        -0.67
    redox     pe
```

```
    units     mol/kgw
    density   1
    Al        1e-25
    Na        0.00069
    K         5e-006
    Ca        0.00014
    Br        3.8e-7
    Mg        6.2e-007
    C         0.0002621 CO2(g)   -3.5
    Cl        0.0004039
    S         6.1e-005
    Si        0.00025
    Fe        3e-009
    -water    1 # kg

KINETICS 1-400
                Annite
                -m0       1.125
                -m      1.125
                -parms   8.64 # 2 órdenes menor que la teórica
                -tol      1e-9
                -runge_kutta 6

TRANSPORT
        -cells           400
        -length          1
        -shifts          16000
        -time_step       10000000
        -flow_direction  forward
        -boundary_cond   flux    flux
        -diffc           0.0e-9
        -dispersivity    0.002
        -correct_disp    true
        -punch           1 2 3 4 5 6 7 8 9 10 15 20 30 40 50 60 70 80 90 100
                         120 140 160 180 200 250 300 350 400
        -punch_frequency 15
        -print           1 400
        -print_frequency 1000

SELECTED_OUTPUT
        -file ref_case_Slong_bis.sel
        -totals Na Mg K Fe Si Cl Ca S C Br Al
        -molalities O2
        -equilibrium_phases calcite kaolinite chalcedony dolomite hematite
        -kinetic_reactants      Annite
        -saturation_indices hematite calcite O2(g) Annite
```